TU Delft

Delft University of Technology

Comparative analysis of hydrological impacts from climate and land use/land cover changes in a lowland mesoscale catchment

Ali, Muhammad Haris; Bertini, Claudia; Popescu, Ioana; Jonoski, Andreja

DOI
10.1080/15715124.2025.2454692

Publication date
2025

Document Version
Final published version

Published in
International Journal of River Basin Management

Citation (APA)
Ali, M. H., Bertini, C., Popescu, I., & Jonoski, A. (2025). Comparative analysis of hydrological impacts from climate and land use/land cover changes in a lowland mesoscale catchment. *International Journal of River Basin Management*. https://doi.org/10.1080/15715124.2025.2454692

Important note
To cite this publication, please use the final published version (if applicable).
Please check the document version above.

Copyright
Other than for strictly personal use, it is not permitted to download, forward or distribute the text or part of it, without the consent of the author(s) and/or copyright holder(s), unless the work is under an open content license such as Creative Commons.

Takedown policy
Please contact us and provide details if you believe this document breaches copyrights.
We will remove access to the work immediately and investigate your claim.

This work is downloaded from Delft University of Technology.
For technical reasons the number of authors shown on this cover page is limited to a maximum of 10.

International Journal of River Basin Management

ISSN: (Print) (Online) Journal homepage: www.tandfonline.com/journals/trbm20

Comparative analysis of hydrological impacts from climate and land use/land cover changes in a lowland mesoscale catchment

Muhammad Haris Ali, Claudia Bertini, Ioana Popescu & Andreja Jonoski

To cite this article: Muhammad Haris Ali, Claudia Bertini, Ioana Popescu & Andreja Jonoski (30 Jan 2025): Comparative analysis of hydrological impacts from climate and land use/land cover changes in a lowland mesoscale catchment, International Journal of River Basin Management, DOI: 10.1080/15715124.2025.2454692

To link to this article: https://doi.org/10.1080/15715124.2025.2454692

© 2025 The Author(s). Published by Informa UK Limited, trading as Taylor & Francis Group

View supplementary material

Published online: 30 Jan 2025.

Submit your article to this journal

Article views: 155

View related articles

View Crossmark data

Full Terms & Conditions of access and use can be found at
https://www.tandfonline.com/action/journalInformation?journalCode=trbm20

INTERNATIONAL JOURNAL OF RIVER BASIN MANAGEMENT
https://doi.org/10.1080/15715124.2025.2454692

Taylor & Francis
Taylor & Francis Group

OPEN ACCESS Check for updates

Comparative analysis of hydrological impacts from climate and land use/land cover changes in a lowland mesoscale catchment

Muhammad Haris Ali [a,b], Claudia Bertini [a], Ioana Popescu [a,b,c] and Andreja Jonoski [a]

[a]Department of Hydroinformatics and Socio-Technical Innovation, IHE Delft Institute for Water Education, Delft, The Netherlands; [b]Water Resources Section, Faculty of Civil Engineering and Geosciences, Delft University of Technology, Delft, The Netherlands; [c]Faculty of Civil Engineering, Politechnica University of Timișoara, Timișoara, Romania

ABSTRACT

The hydrological processes within the catchment are generally influenced by both climate change (CC) and land use/land cover (LULC) change. However, most of the studies are focused on their individual impact on the catchment's hydrology, while their combined effects have received little attention. This study employs the physically based distributed hydrological model, MIKE SHE, to study the separate and combined effect of climate and LULC change on the hydrology of a mesoscale catchment in the near future (2050s). An Artificial Neural Network – Cellular Automata (ANN-CA) based prediction model was trained to simulate the future LULC map. The future meteorological data under four CC scenarios was obtained from the Royal Netherlands Meteorological Institute (KNMI). The model results showed that the combined effects of CC with LULC changes did not significantly differ from the individual impact of CC on the catchment scale. However, on the local scale, the changes in LULC can significantly influence the variations in groundwater table, soil moisture, and actual evapotranspiration ranging from approximately – 6–15%, – 9–27%, and – 30–10% respectively, depending on the specific change in LULC class and season. In summary, this research provides valuable insights into the complex interactions between LULC changes, CC, and hydrology.

ARTICLE HISTORY
Received 26 June 2024
Accepted 13 January 2025

ASSOCIATE EDITOR
Kory Konsoer

KEYWORDS
ANN-CA; future LULC prediction; MIKE SHE; KNMI'23 climate scenarios; Aa of Weerijs catchment; climate change

1. Introduction

Climate change poses serious risks to water availability and food security, impeding progress towards Sustainable Development Goals. Its far-reaching adverse effects influence both natural ecosystems and human communities, revealing disparities across different systems, regions, and sectors (Lee *et al.* 2024). The IPCC Sixth Assessment Report (AR6 2023) stated with a high degree of confidence that the rate of rise in global surface temperature since 1970 has surpassed that of any other 50-year period in the past 2000 years. This continuous temperature rise underscores the increasingly apparent climate-driven changes (Blöschl *et al.* 2019).

Climatic variations, particularly changes in precipitation and temperature, can profoundly affect both the hydrological state and the spatiotemporal distribution of water resources (Sorribas *et al.* 2016; Sunde *et al.* 2017). To counter these, water management strategies need to prioritise climate change, emphasising the implementation of basin-scale hydrological management techniques (IWMI 2019). However, selecting appropriate adaptation strategies necessitates a thorough understanding of the potential impact of global climate change on the local environment (Adib *et al.* 2020). Therefore, one of the initial steps in assessing the impact of climate change on hydrological systems involves comprehending how future climate signals will influence key catchment hydrological variables.

Alongside climate change, land use/land cover (LULC) change is also one of the important drivers of hydrological variations (Rigby *et al.* 2022; Kundu *et al.* 2017; Trang *et al.* 2017). Changes in LULC can influence hydrological processes, such as evapotranspiration (ET), interception, infiltration, and surface runoff. These effects occur through direct alterations to the landscape's morphology and physiology, as well as indirect modifications to the soil and atmospheric boundary layers (Zhang *et al.* 2018).

Research examining the impact of human-induced changes in landscape patterns and climate change has gathered significant attention. However, the majority of this research has primarily focused on either the effects of climate change or changes in land use, rather than considering both factors combined (Nazeer *et al.* 2022; Gurara *et al.* 2021; Kay *et al.* 2021; Adib *et al.* 2020). In addition to that, when these factors are examined together, the emphasis of the study is often centred on evaluating variations in surface hydrological variables alone (Ma *et al.* 2023; Lyu *et al.* 2023; Zhang *et al.* 2023; Sinha *et al.* 2020; Iqbal *et al.* 2022) or only on groundwater dynamics (Hanifehlou *et al.* 2022; Ghimire *et al.* 2021).

Furthermore, the existing literature presents a certain level of variation regarding the individual influence of climate change and LULC change on hydrology. While some studies assert that LULC change had a more significant impact on hydrological variables in their study areas (Zhang *et al.* 2023; Zhou *et al.* 2019), others highlighted

CONTACT Muhammad Haris Ali m.h.ali@tudelft.nl Department of Hydroinformatics and Socio-Technical Innovation, IHE Delft Institute for Water Education, P.O. Box 3015, Delft 2601 DA, The Netherlands; Water Resources Section, Faculty of Civil Engineering and Geosciences, Delft University of Technology, Delft 2628 CD, The Netherlands

Supplemental data for this article can be accessed online at https://doi.org/10.1080/15715124.2025.2454692.

© 2025 The Author(s). Published by Informa UK Limited, trading as Taylor & Francis Group
This is an Open Access article distributed under the terms of the Creative Commons Attribution License (http://creativecommons.org/licenses/by/4.0/), which permits unrestricted use, distribution, and reproduction in any medium, provided the original work is properly cited. The terms on which this article has been published allow the posting of the Accepted Manuscript in a repository by the author(s) or with their consent.

the prominent influence of climate change (Huq and Abdul-Aziz 2021; Ye *et al.* 2023; Iqbal *et al.* 2022; Fu *et al.* 2019). Consequently, a dedicated combined analysis for a specific catchment becomes imperative (Wedajo *et al.* 2022). Further, the positive or negative change in the climatic variables due to climate change is quite uncertain as the Global Climate Models (GCM)/Regional Climate Models (RCM) differ for each study site, along with climate and land use characteristics (Blöschl *et al.* 2019; Song *et al.* 2021). Hence, conducting a study for the area of interest with a focus on local changes is seen as crucial for a comprehensive assessment of catchment surface and subsurface hydrological changes, which is necessary for the development of effective water management practices.

In recent years, nearly all regions of Europe have experienced significant impacts from droughts affecting critical systems such as agriculture, water supply, energy, river transport, and ecosystems. These impacts are projected to intensify further attributed to climate change (Rossi *et al.* 2023). In the summer of 2018, the Netherlands experienced below average precipitation during May, June, July, September, and October. The Southern and Eastern regions of the country were more affected by this dry period, leading to significant impacts on crop yield and grasslands due to a reduction in water availability (Philip *et al.* 2020). The situation was similar in the Aa of Weerijs catchment, which is situated in the south of the Netherlands and shared with Belgium. The main land use in the area is agriculture, which highly depends on water resources. It is important to analyse the future local hydrological trends in the catchment to prepare for long term effective management practices in the area. Therefore, focusing on this catchment, this paper aims to analyse both the individual and combined impacts of future projected changes in LULC and meteorological variables on surface and subsurface hydrology. Additionally, it seeks to address a knowledge gap about how crucial is it to consider future LULC changes alongside changes in meteorological variables under climate change when assessing the future hydrological state of a mesoscale (346 km^2) catchment. To conduct the analysis, a fully distributed hydrological model using MIKE SHE modelling tool was setup with historical data. The simulation results were then compared by running the model with: future meteorological data from KNMI'23 climate scenarios alone, with only the ANN-CA predicted future LULC map, and with both combined.

Following this introduction, the paper provides an overview of the study area and details the research materials and methods utilised. Subsequently, the results obtained from the research are presented, along with a comprehensive discussion of the findings. Finally, the paper concludes with a summary of the key findings and their implications.

2. Materials and methods

2.1. Study area

The chosen study area for this research is the Aa of Weerijs, a transboundary mesoscale catchment shared between the Netherlands and Belgium. It covers an area of 346 km² out

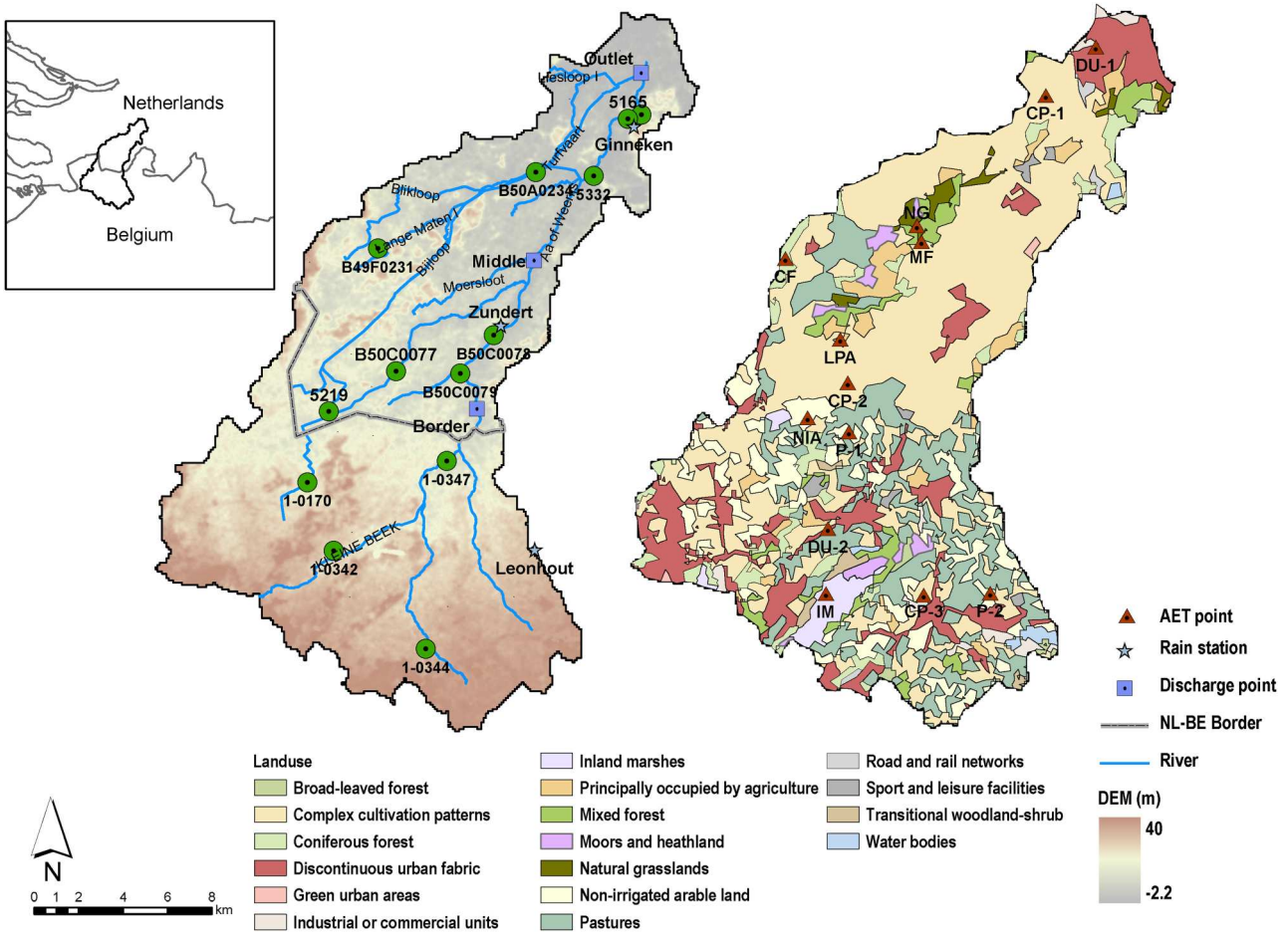

Figure 1. Location of the study area, river network, elevations (CLMS n.d.-a) and LULC (CLMS n.d.-b). The map also shows the discharge, groundwater, and AET locations where the model performance has been evaluated. The abbreviations used for AET locations represent the LULC, according to the following convention: CP: Complex cultivation pattern; DU: Discontinuous urban fabric; NIA: Non-irrigated arable land; LPA: Land principally occupied by agriculture; CF: Conifer forest; NG: Natural grassland; IM: Inland marshes; MF: Mixed forest; P: Pastures.

of which approximately 147 km^2 is located in the Netherlands. The main stream originates in the region of Brecht, Belgium, and flows towards the outlet near Breda, the Netherlands, where it enters the city canals and eventually joins River Mark (Figure 1).

It is a lowland catchment, mostly flat with a gentle slope of approximately 0.5% (de Klein and Koelmans 2011). In the last five decades of the twentieth century, the area underwent many alterations to adapt to the changing demands of urbanisation and agriculture. The streams and channels were normalised and the drainage network was intensified to reclaim the land (Witter and Raats 2001). Almost no remnants of the original swamps remain.

Based on the in-situ gauged data from 2010 to 2020, the average annual gross rainfall in the area is approximately 850 mm y^{-1}, resulting in approximately 249 mm y^{-1} flow at the catchment's outlet. The modest value of the runoff ratio (30%) suggests a high level of water consumption within the catchment. The main land use in the area is agriculture and pastures. According to the Corine Land Cover (CLC) 2018 (CLMS n.d.-b), the agriculture area comprises around 72.8% of the total area. Built-up areas cover 13.6%, while forest and natural grassland areas collectively cover 9.3% which are mainly located along the Bijloop and Turfvaart channels.

In the catchment, sandy soils are the main soil type and are characterised by sand-covered ridges with streams typically deeply incised within them. In recent years, the catchment is facing challenges regarding water shortages during the summer season. This is attributed to the degradation of subsurface soil, affecting water retention and canal networking. Various factors exacerbate this situation, including climate change, growing demand for water in the tree-nursery export sector, and hot dry summers. These pressures are intensifying, compounded by the simultaneous high demand for protected and dedicated nature and recreation areas expressed by the residents of Breda, Zundert, and Roosendaal (Beers *et al.* 2018). Given the prevailing conditions, it is crucial to analyse how the future climate conditions and LULC changes will impact the hydrology of the catchment.

2.2. Model setup and data

To achieve the objectives of the study, a fully distributed physically based hydrological model has been set up using the MIKE SHE (Systeme Hydrologique Europeen) modelling tool developed by the Danish Hydraulic Institute (DHI), Denmark. It contains physics-based modules on overland flow (2D Saint-Venant equation, Popescu 2013), unsaturated zone (1D Richards' equation, Richards 1931), groundwater (3D Boussinesq equation, Boussinesq 1904), and fully dynamic channel flow, incorporating complex interactions and feedback between these modules. It uses a finite difference approach to solve the partial differential equations describing these processes (Thompson *et al.* 2004). It has the capacity to simulate all significant processes of the hydrological cycle (Refsgaard *et al.* 2010) and the capability to simulate integrated surface-subsurface hydrology more efficiently, especially in flat areas characterised by dense river networks and shallow groundwater, by employing physically based methods, in contrast to conceptual models like Soil and Water Assessment Tool (SWAT) that rely on empirical equations for simulating interactions (Ma *et al.* 2016).

For the study area, the model was set up for the period 15-09-2009–31-12-2019. The initial three-and-a-half-months were used as a model spinning up period. Calibration was conducted for the years 2010–2016, while validation was performed for the years 2017–2019. For meteorological forcing data, daily rainfall data at two stations situated in the Netherlands (Ginneken and Zundert, marked in Figure 1) was sourced from the Royal Netherlands Meteorological Institute (KNMI n.d.). The data for the third station (Leonhout, marked in Figure 1) located in Belgium was obtained from the Flemish Environment Agency (VMM n.d.). These stations are all located towards the Eastern side of the catchment, as no rain gauges are available in the West side of the catchment. In general, a uniform spatial distribution of rain gauges ensures a better representation of rainfall and its variability over wide areas. In this research, however, the catchment itself is small (346 km^2) and relatively flat, which reduces the potential of significant spatial variability in meteorological data. Moreover, the average rainfall on these stations is in close range (Ginneken: 2.3 mm d^{-1}, Zunder: 2.3 mm d^{-1} and Leonhout: 2.2 mm d^{-1} for the period 2010-2019), which shows that the spatial variability of rainfall in the catchment is limited and these stations can describe the rainfall distribution over the catchment reasonably well. There are many interpolation techniques available for upscaling rainfall data from point observations for representing over the model domain. However, each technique has its advantages and limitations (Hofstra *et al.* 2008). Considering the relatively flat topography of the catchment, the rainfall was presented over the model domain using Thiessen polygons as it is reported as simple and robust method (Liu *et al.* 2017).

The daily Potential ET (PET) data was obtained from the closest weather station (Gilze Rijen) located in the Netherlands towards the North-East side of the catchment and provided as spatially uniform over the entire grid in the model. We acknowledge that PET varies depending upon topography, soil and vegetation cover characteristics but the due to small size of the catchment and relatively flat terrain, PET is expected not to vary considerable with topography. The variations of land (vegetation) cover are taken into account when calculating actual evapotranspiration using varying vegetation parameters (root depth, leaf area index etc.). An alternative option to the use of uniformly distributed PET over the catchment was to obtain PET data from Earth observation gridded products, but these datasets have many associated uncertainties and cannot be regarded as actual observations (Rajib *et al.* 2018; Ali *et al.* 2023). Therefore, to avoid any additional uncertainties and ambiguities, PET data from the weather station was provided as spatially uniform over the entire grid in the model.

The topography in the model was represented using elevation data from EU-DEM version 1.1 (resolution: 25 m, CLMS n.d.-a), while the LULC was represented using CLC 2018 (resolution: 100 m, CLMS n.d.-b). The data on vegetation characteristics, including Leaf Area Index (LAI) and root depth was acquired from the National Hydrologic Instrumentation (NHI) sub-report on crop characteristics (NHI 2008). The values of Manning's roughness coefficient corresponding to CLC classes were used from the study of Papaioannou *et al.* (2018).

The grid resolution of MIKE SHE model was set as 500 m. The selected grid resolution reflects a compromise between computational efficiency and the need for spatial

detail in representing the modelled parameters and processes. Finer resolutions can capture smaller-scale spatial variability but they would significantly increase computational time without proportionate improvement in model's accuracy (Vazquez *et al.* 2002). Importantly, the catchment is not flood prone, so the chosen resolution is sufficient for simulating the river and surrounding catchment dynamics effectively while allowing for reasonable simulation times, as supported by similar studies in the literature (Loliyana and Patel 2020). Further compared to lumped or semi-distributed hydrological models where often each sub catchment is represented as a single unit, 500 m grid cell provides much greater spatial detail. The main tributary of the river network, the Aa of Weerijs, has an average bed width of approximately 10 metres. The routing within the river is modelled using MIKE 11, with its geometry defined through detailed cross-sectional data. The exchange between MIKE 11 and MIKE SHE occurs at each grid cell, based on the dynamic relationship between river water levels and groundwater levels at those cells after each computational time step. Therefore, the selected grid cell size did not affect the representation of river and flow routing process.

The data of the river cross-sections was obtained from the water authority of the Dutch part of the catchment, the Water Board Brabantse Delta (WBD). A discharge of 0.03 m^3s^{-1} was set as upstream boundary condition to ensure numerical stability by preventing drying conditions. All streamflow is subsequently generated through interactions between MIKE 11 river component and the MIKE SHE grid cells. A rating curve was provided as a downstream boundary condition. The Manning's roughness coefficient value was provided as 0.03 (Chow 1959). The model incorporated the primary 29 weirs, out of which 7 were automated. The crest levels and target upstream water levels for the automated weirs were also provided by WBD. The model integrated these specified gate operation values for weirs to account for flow regulation.

For the unsaturated zone, the method based on the Richards equation was selected for the simulation of processes. It was characterised using soil texture data obtained from the 'Land Use/Land Cover Area Frame Survey' (LUCAS) 2015 topsoil physical properties dataset (Ballabio *et al.* 2016). According to this dataset, five different soil textures are present in the area. These soils were further categorised based on soil carbon content data (LUCAS topsoil chemical properties dataset, Ballabio *et al.* 2019), resulting in a soil map with 18 classes. The hydraulic soil properties were defined were defined using the van Genuchten method (van Genuchten 1980), values were calculated using pedotransfer function equations from Wösten *et al.* (1999).

For the saturated zone, the MIKE SHE implemented 3D Finite Difference method was selected and it was considered as an 80 m deep single aquifer layer. The boundary condition was set as spatially distributed fixed heads along the boundary, with values representing the average groundwater levels along the boundary from 2009 to 2016. Saturated horizontal hydraulic conductivity values were sourced from the Netherlands REGIS II V2.2 hydrogeological model (Gunnink *et al.* 2013; Vernes *et al.* 2005). These values were extended to the Belgian part of the catchment through interpolation. Small streams and ditches having an average bed width less than 1 m were not modelled in MIKE 11 but were incorporated into the model using the conceptual drainage component of MIKE SHE. Their levels were set equal to the average bed levels of these small drains with in each model grid.

For model calibration (2010-2016), a manual, one-at-a-time approach was employed. Given the physically based nature of the model, most parameter values were derived either from field data or existing literature. Consequently, only limited parameters were considered for calibration. These were drainage time constant, specific storage, and specific yield. Among the considered parameters, drainage time constant proved to be the most sensitive concerning the simulation of groundwater levels. Nash-Sutcliffe Efficiency coefficient (NSE) and Correlation coefficient (R) were used as evaluation matrices. The target variables included streamflow at 3 locations, groundwater levels at 11 locations, and actual ET (AET) at 13 locations (Figure 1). During the validation (2017-2019), the same variables were considered, except for two groundwater locations (B49F0231 and B50A0234) due to data unavailability. In this paper, the term 'groundwater level' (GWL) is employed when referring to levels with respect to the Amsterdam Ordnance Datum (NAP), while 'groundwater table' (GWT) is used when referencing levels with respect to the surface. A summary of the data sets used to set-up the model in historical conditions (2010-2019) is presented in Table 1.

2.3. Future land use / land cover projection

LULC plays an important role in hydrology as changes in it can disturb water and energy balances consequently affecting processes such as transpiration, interception, evaporation, and infiltration. The impact of future LULC can be assessed

Table 1. Datasets used for model setup and performance evaluation.

Data	Temporal resolution	Spatial resolution	Source
Rainfall	Daily	Point data	NL: Ginneken, Zundert (KNMI n.d.); BE: Leonhout (VMM n.d.)
Potential evapotranspiration	Daily	Point data	Gilze Rijen Weather station (KNMI n.d.)
Vegetation parameters (LAI and root depth)	–	–	NHI (2008)
Actual evapotranspiration	Daily	100 m	Satellite-based evaporation data for the Netherlands SATDATA 3.0 (Meteobase n.d.)
Observed groundwater levels	Daily, Bi-weekly	Point data	NL: WBD, DINOloket (n.d.) BE: DOV (n.d.)
Observed discharge	Daily	Point data	WBD
River geometric data	–	–	WBD
Topography	–	25 m	European Digital Elevation Model (EU-DEM v1.1, CLMS n.d.-a)
Land use land cover	–	100 m	Corine Land Cover (CLC 2018, CLMS n.d.-b)
Soil texture and typology	–	500 m	LUCAS 2015 topsoil physical properties dataset (Ballabio *et al.* 2016)
Soil carbon content (%)	–	500 m	LUCAS topsoil chemical properties dataset (Ballabio *et al.* 2019)

Acronyms used in the table: NL: Netherlands; BE: Belgium; LAI: Leaf area index; WBD: Water Board Brabantse Delta; DOV: Databank subsurface Flanders; LUCAS: Land Use/Land Cover Area Frame Survey

in two ways. The first option involves considering a hypothetical scenario where one LULC type undergoes a complete transformation into another type (Zhang *et al.* 2020). This approach is, however, subjective and lacks specificity. Alternatively, the impact can be evaluated by simulating future LULC using prediction models based on past changes and other influencing variables (Getachew *et al.* 2021). These prediction models generally use techniques such as Cellular Automata (CA), the Markov Chain Model (Marhaento *et al.* 2018), and Artificial Neural Networks (ANN). CA is a commonly used method that predicts the evolution in LULC based on the initial state, neighbouring cells, and transition rules. Complicated transition rules are often defined by coupling neural networks with CA (Liu *et al.* 2017). Machine learning algorithms can facilitate the learning of change factors based on historical data from two periods to simulate the change rules for future maps.

In this study, ANN-CA was used to simulate the potential future LULC map because of its consistently satisfactory performance over the literature (Roy and Rahman 2023; Kafy *et al.* 2020). For this task, we utilised QGIS 2.18 and the MOLUSCE plugin. Given the availability of CLC maps for the earliest (1990) and most recent (2018) years, the subsequent predicted map was generated for the year 2046 considering it as a representation of the average LULC condition of the catchment in the 2050s. The process involved two phases. In the first phase, CLC maps for 2006 and 2012 were treated as dependent variables, while raster maps of Euclidean distance from rivers, roads, and digital elevation served as independent variables. The dependent variables were used by the tool to calculate pixel-by-pixel change map while Pearson correlations are calculated between independent variables. The Multilayer Perceptron (MLP) ANN was then trained to predict transition potential. Afterward, CA was employed to simulate the LULC map for 2018, which was validated against the CLC map for that year. The finest results were achieved with parameter values of learning rate = 0.10, hidden layers = 1 with 10 neurons, momentum = 0.050, and iterations = 1000. The kappa coefficients ($k_{overall}$, k_{histo}, and k_{loc}) and percentage of correctness were used to quantify the agreement between the reference and simulated LULC map.

In the second phase, using the above mentioned finalised parameters of the model, the map for 2046 was simulated using the CLC maps from 1990 and 2018, along with the aforementioned independent variables. It is worth mentioning here that the future map was simulated under a business-as-usual scenario, without incorporating any landscape planning policies or restrictions on specific LULC classes. The study's objective was not to generate various future landscapes but to find out the hydrological significance of incorporating future LULC maps in climate change studies. Therefore, the business-as-usual scenario was chosen to generate the future LULC map assuming it as a representative of a worst-case scenario.

2.4. Future meteorological projections

To run the hydrological model for future climate change analysis, rainfall, and potential evapotranspiration (PET) data are required. For this study, the future climate data is obtained from KNMI (Koninklijk Nederlands Meteorologisch Instituut), the meteorological institute of the Netherlands. The dataset is known as KNMI'23 climate scenarios, as it was made publicly available in October 2023. These scenarios are based on the Coupled Model Intercomparison Project (CMIP6) model runs and translate the Intergovernmental Panel on Climate Change (IPCC) 2021 global climate projections for the Netherlands. The KNMI's Global Circulation Model (GCM) EC-Earth3 model, which is also part of Coupled Model Intercomparison Project (CMIP6) models, was re-tuned to reduce the bias and resampled based on CMIP6 target values. The results were then dynamically downscaled with the regional atmospheric climate model RACMO, also owned by KNMI. In the end, the outputs of RACMO were bias-corrected based on observed data (1991-2020) using the Quantile Delta Mapping method (Cannon *et al.* 2015). More details can be found in the scientific report by KNMI (van Dorland *et al.* 2023).

KNMI'23 scenarios consist of six paths that describe the possible future climate in the Netherlands around the years 2050, 2100, and 2150. In this study, we are focused only on the near future (2050). For that time frame, the climate scenarios data is available from 2036 to 2065, with the 30-year time horizon representing the averaging condition of 2050. The scenarios are based on the three levels of CO_2 emissions, according to the Shared Socioeconomic Pathways (SSP): high 'H' (SSP5-8.5), moderate 'M' (SSP2-4.5), and low 'L' (SSP1-2.6). Each emission scenario is further combined with wetting scenario 'N' ('Wet' is 'Nat' in Dutch) and drying scenario 'D' ('Dry' is 'Droog' in Dutch) based on the circulation of precipitation. The wetting scenario represents a wetting trend in winter and moderate drying in summer, while the drying scenario provides drier conditions in summer and moderate wetting in winter. Consequently, the six resulting scenarios are HN, HD, MN, MD, LN, and LD.

In this study, scenarios MN and MD were not considered due to our focus on extreme climate change scenarios. Our analysis concentrated on the high CO_2 emissions scenarios (HN, HD) and low CO_2 emissions scenarios (LN, LD). Moreover, as scenarios MN and MD lie between the high and low envelopes, their elimination did not affect the high and low values of the results. The data at the daily time step is available at a resolution of 0.5° by 0.65° and covers only the Dutch part of the catchment. To overcome this issue, the model grids belonging to the Belgian part of the catchment were filled with data from the closest neighbouring grid cells. The time series were extracted from the gridded data at the locations where the three rain stations (Ginneken, Zundert, and Leonhout) are situated (Figure 1) and presented interpolated over the model domain using Thiessen polygons to keep the methodological consistency with the base model.

Moreover, the future projected rainfall and PET for the time horizon 2050 (2036-2065) were compared with observed data from the base period (2011-2020) to calculate the projected relative change in rainfall and PET. To analyse extreme events, the statistical metric 'R95pTOT' was calculated for each season using catchment average rainfall data for the base period and future scenarios. R95pTOT quantifies the contribution of very wet days to the total rainfall, with the threshold for very wet days set at the 95th quantile of daily rainfall data for the base period. It is also defined as the sum of rain in wet days, i.e. days with rainfall above the 95th percentile. Further, the rainfall duration curves were

Table 2. Description of designed simulation scenarios.

Abbreviation	Meteorological data	LULC map
SC1	Observed data for base period (2010-2019)	2046
SC2	Climate scenarios LD, LN, HD, and HN for 2050-time horizon (2036-2065)	2018
SC3	Climate scenarios LD, LN, HD, and HN for 2050-time horizon (2036-2065)	2046

plotted to compare the low, middle, and high-intensity rainfall events for the base period and four climate projection scenarios. The 95th and 30th percentile lines were marked as thresholds for comparison of high and low intensity rainfall events (Jian *et al.* 2022).

2.5. Simulation scenario design

To assess the impacts of climate change and LULC change on the hydrology of the Aa of Weerijs catchment and to elucidate the significance of incorporating future LULC considerations in climate change studies, three simulation scenarios were developed. The first scenario exclusively considered future LULC changes, obtained with the developed ANN-CA model. The second scenario solely accounted for changes in future meteorological variables and employed the developed MIKE SHE model forced with the KNMI'23 climate projections. The third scenario, instead, considered both future LULC and climate change. Further details are provided in Table 2.

To analyse the results under these scenarios, the relative changes in seasonal catchment averages for AET, discharge at the catchment outlet, recharge to groundwater (recharge), and base plus drain flow to the river (subsurface flow) were computed using Eq. (1).

$$\Delta = \frac{X_{scenario} - X_{base}}{X_{base}} \times 100 \quad (1)$$

where Δ represents relative change, X_{base} is the variable value simulated during the base period and $X_{scenario}$ is the variable simulated under the respective scenario. A positive value of Δ indicates an increase while a negative value indicates a decrease. For the GWT, as the levels are referenced to the surface, the terms in the numerator of Eq. (1) were inverted to maintain consistency in sign conventions.

The results were further examined at the local level, considering seasonal spatially distributed values for AET, soil moisture (SM) in the top 10 cm layer, and GWT using Eq. (1) at each grid cell, and results are presented as maps.

3. Results and discussion

3.1. Future land / use land cover simulation

CLC maps of the years 1990 and 2018, along with other driver variables such as Euclidean distance from rivers, roads, and DEM, were used to simulate the future LULC map of the year 2046 using the developed ANN-CA model. Before simulating the future LULC map, the LULC prediction model was validated using the CLC 2018 map. The agreement between the reference and simulated map was assessed using the kappa coefficients ($k_{overall}$, k_{histo}, k_{loc}) and the percentage of correctness. Their values were 0.94, 0.97, 0.95, and 95.7% respectively, lying in the high agreement range (Roy and Rahman 2023; Viera and Garrett 2005). The map of 2046 was then simulated using the validated model (Figure S1 of supplementary material).

According to the CLC map, the area was categorised into 17 different land use classes, which were aggregated into 5 major classes following Feranec *et al.* (2016) for understanding the major shifts in the LULC (Table 3). According to the results, the built-up area has shown a consistent increase over the examined period. Starting at 39 km² (11.3%) in 1992, it expanded to 47 km² (13.6%) in 2018 and is projected to further grow to 52.8 km² (15.3%) by 2046. This pattern reflects further urbanisation and infrastructure development in the area. Agricultural lands experienced a minor decrease from 263.3 km² (76.1%) in 1992 to 251.8 km² (72.8%) in 2018. The map of 2046 suggested a continued decline to 244.5 km² (70.7%) but still agriculture remained the dominant LULC in the region. Considering the changes within the agricultural class of landcover, 1.75 km² of area has been projected to shift from 'Complex cultivation patterns' (CCP) to 'Land principally occupied by agriculture' (LPA). The category of 'Forest and semi-natural' (FSN) areas demonstrated minor positive growth, increasing from 38.3 km² (11.1%) in 2018 to 39.8 km² (11.5%) in 2046. Wetlands remained relatively stable over the years. Starting at 6.8 km² (2%) in 1992, they decreased slightly to 6.5 km²

Table 3. Areas under historical (1990, 2018) and future simulated (2046) LULC maps.

		Historical				Simulated	
		1990		2018		2046	
Corine land use / land cover class	Aggregated class	km²	%	km²	%	km²	%
Discontinuous urban fabric Industrial or commercial units Road and rail networks and associated land Green urban areas Sport and leisure facilities	Built-up area	39	11.3	47	13.6	52.8	15.3
Non-irrigated arable land Pastures Complex cultivation patterns Land principally occupied by agriculture, with significant areas of natural vegetation	Agricultural	263.3	76.1	251.8	72.8	244.5	70.7
Broad-leaved forest Coniferous forest Mixed forest Natural grasslands Moors and heathland Transitional woodland-shrub	Forest and semi-natural	34.8	10.1	38.3	11.1	39.8	11.5
Inland marshes	Wetlands	6.8	2	6.5	1.9	6.5	1.9
Water bodies	Water bodies	2	0.6	2.3	0.7	2.3	0.7

(1.9%) in 2018, but the projected map maintained this stability at 6.5 km² (1.9%) in 2046. Similarly, for the water bodies, the simulated covered area remained 2.3 km² (0.7%).

In general, there has not been any unrealistic LULC change in the region which is predicted by the ANN-CA model. The simulated map for the year 2046 indicated an expansion of built-up areas, particularly around existing urban zones, encroaching into agricultural areas. It is important to note that the simulated future map for the year 2046 was generated under a business-as-usual scenario, without the integration of specific landscape planning policies or restrictions on LULC classes. The choice of a business-as-usual scenario serves as a representation of a worst-case scenario, emphasising the potential impacts of unchecked urban expansion and changes in agricultural land use. By doing so, the study aims to highlight the hydrological consequences associated with the absence of proactive planning measures or land management policies in the face of future climate and LULC changes. This approach provides valuable insights into the potential challenges and risks that may arise under such conditions, contributing to a more comprehensive understanding of the complex interactions between land use, climate, and hydrology.

3.2. Future meteorological projections

The 10 years from 2010 to 2019 were considered as a baseline period to calculate the relative change (Eq. 1) as a percentage difference for rainfall and PET, for the assessment of projected meteorological changes in the 2050 horizon. The outcomes of the comparison across all scenarios are presented in a range based on the highest and lowest values achieved overall. The findings indicated that in all months the percentage change in PET is positive under each scenario, indicating an increase in future conditions. In contrast, rainfall exhibited a more random pattern (Figure 2). During winter months (DJF: December, January, February), minor variations in rainfall are observed in January and December. However, In February, the percentage increase ranged from 17.3% to 24%, making it the wettest month in the winter season. In March and April, there is a notable increase in rainfall percentages (ranging from 3.9–14.7% and 6.9–11.3%, respectively) compared to December and January. Conversely, the rise in PET during these months is less pronounced, ranging from 1.6–5.3% and 3.3–6.7%, respectively. The combined effects contribute to making March and April relatively wetter. Conversely, in December and January, the relative percentage differences in rainfall are lower (−1.2–6.6% and – 5.2–2.6%, respectively), while PET shows more substantial increases (ranging from 8–10.1% and 14–15.8%, respectively), leading to relatively low wet conditions. This shift indicates a temporal change in the rainfall pattern, transitioning from the winter months (December and January) to the spring months (March and April), resulting in increased rainfall during the latter period.

The months of May, July, and August show an increase in PET accompanied by a decrease in rainfall. In June, rainfall is projected to decrease by – 1.6% under the HD scenario, while it is expected to increase upto 7.9% in other scenarios with a maximum value under HN scenarios, respectively. However, PET in June is projected to increase under all scenarios by 4.1–8.5%, not balancing the increase in rainfall, likely making the overall conditions drier. August emerges as the driest month, characterised by a rise in PET and a decline in rainfall in the ranges of 12.6–17.3% and 7.9–18.3%, respectively. Moving to autumn (SON: September, October, and November), there is an overall major increase in rainfall compared to other seasons (13–15.5%), but PET also shows an upward trend (Figure 2). Winter also shows an increase in rainfall (2–9.1%) but is accompanied by a simultaneous rise in PET (8.8–10.1%), consequently balancing out the increase in rainfall.

For the rainfall, the results align with the broader consensus that Europe is expected to experience wetter conditions in winter and drier conditions during summers, especially in the Northern part of Europe (e.g. Sassi *et al.* 2019). However, with the temperature rise, PET will also be increasing. The future scenarios indicate that the percentage increase in PET (6.7–10.1%) is more pronounced compared to the rise in rainfall (1.4–6.1%) on an annual scale. This suggests that the catchment may face increased stress in terms of water availability. Moreover, focusing specifically on the summer months (JJA: June, July, August), the findings suggest a tendency for decreased rainfall (3.4–11.3%)

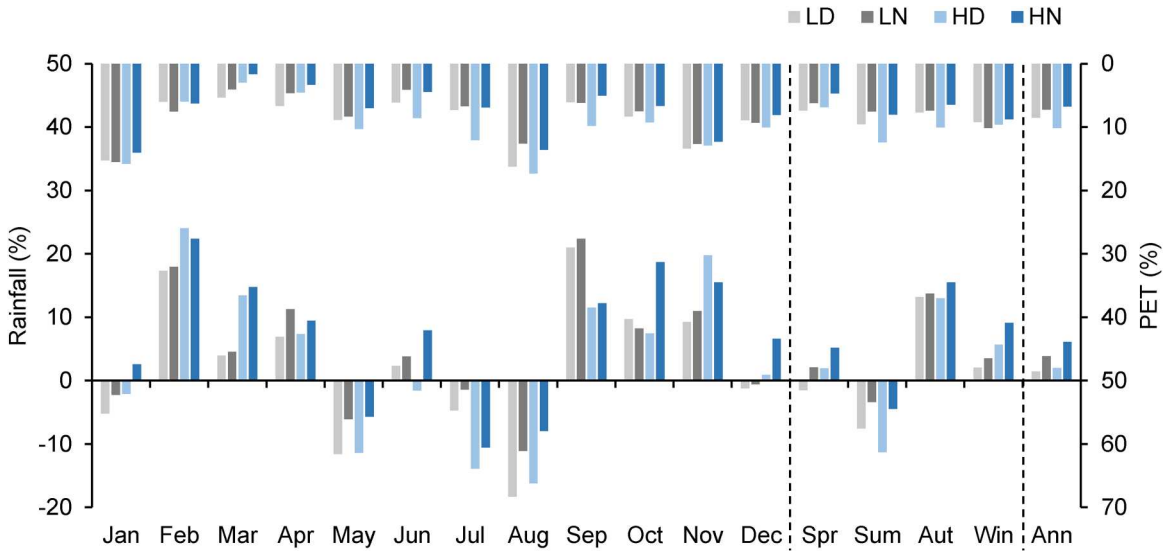

Figure 2. Relative change in rainfall and PET calculated in percentage under the KNMI'23 climate projection scenarios for the time horizon 2050 with reference to the base period. Dashed lines separate the plots that indicate the averages across seasons and annual data (spr: spring, sum: summer, aut: autumn, win: winter, ann: annual).

coupled with a substantial increase in PET (7.5–12.4%). This combination further emphasises the potential for water stress during the critical summer months. The observed increasing trends of PET in the Netherlands are consistent with the findings of Philip *et al.* (2020), wherein the importance of PET in characterising the summer droughts in the Netherlands is highlighted and attributed to changes in atmospheric circulation.

The observed trends regarding the increase ET and decreased precipitation during summer under future climate broadly align with findings from other regions in the Netherlands such as Dommel catchment (van Vliet *et al.* 2012), Keersop catchment (Visser *et al.* 2012) and Veluwe region (Van Huijgevoort *et al.* 2020). To analyse extreme events, the statistical metric 'R95pTOT' was calculated for each season under both the base and future scenarios (Table S1 of supplementary material). During the base period, summer exhibited the highest total rainfall from very wet days, aligning with the findings of Whitford *et al.* (2023). These higher values indicate that the majority of summer rainfall occurs in short periods with high intensity. Conversely, R95pTOT values were lowest in spring. In future climate scenarios, R95pTOT values are notably low, suggesting a decrease in the intensity of extreme events and a shift towards more events with a lower intensity of rainfall.

This observation was further analysed by plotting duration curves for both the base and future scenarios using daily rainfall and their corresponding exceedance probability (Figure 3). While there is minimal difference between the duration curves of the four future scenarios, a comparison between the base period and future scenarios indicates a decrease in high rainfall events under all scenarios, accompanied by a significant increase in low rainfall events. Days with rainfall greater than approximately 2.2 mm are decreasing, while days with lower rainfall are increasing. This result, however, is potentially influenced by the different nature of the in-situ data used for the base period, i.e. point-based, and of the climate projections, i.e. grid-based. Indeed, rain gauges, strategically positioned on the ground, are designed to measure precipitation at specific locations which enable them to capture localised events like heavy downpours. In contrast, future scenarios are the climate model outputs that operate on a broader spatial scale where each grid cell represents an averaged value for climate variables, providing a more generalised view over larger regions but also less capabilities in representing extremes.

3.3. Model calibration and validation

For the catchment average AET, the values of R and NSE for the calibration and validation periods were 0.91, 0.80, 0.926, and 0.822, respectively. Figure S2 (supplemental material) shows that the catchment average observed and simulated AET exhibit good agreement. The values of NSE and R at all locations for the calibration and validation period are provided in Table S2 of the supplemental material.

In terms of discharge at the catchment outlet, NSE and R values during calibration and validation were 0.88, 0.71, 0.87, and 0.71, respectively. While the model tended to underestimate the magnitude of high peaks, the plots in Figure S3 (supplemental material) demonstrate the reasonable capture of trends during both high and low flow periods, indicating the model's ability to reflect seasonal variations adequately.

The simulation of GWLs showed varying model efficacy across different locations. The plots of groundwater levels at four locations are presented in Figure S4. The model tended to slightly overestimate the GWLs in the upstream regions and around the catchment's outlet. Nevertheless, the model results demonstrated good agreement with observed data for GWLs, capturing seasonal variations and trends reasonably well ($R = 0.77$ for the average of all observed versus modelled outputs).

3.4. Impact on catchment hydrology under designed scenarios

3.4.1. Scenario SC1, under future LULC changes

In scenario SC1, the model was simulated for the base period 2010–2019 using a future LULC map (2046) to assess the individual effects of LULC changes on the catchment's hydrology. The impacts have been assessed on various simulated variables, including discharge at the catchment outlet, AET, subsurface flow, and recharge at the catchment scale. In addition, the impacts on AET, GWT, and SM (top 10 cm) were evaluated at the local scale as well.

Under the future LULC change, the effects on hydrology at the catchment level are minimal. The mean monthly discharge is almost the same as the base model with a minor increase (Figure 4). The maximum observed increase occurs

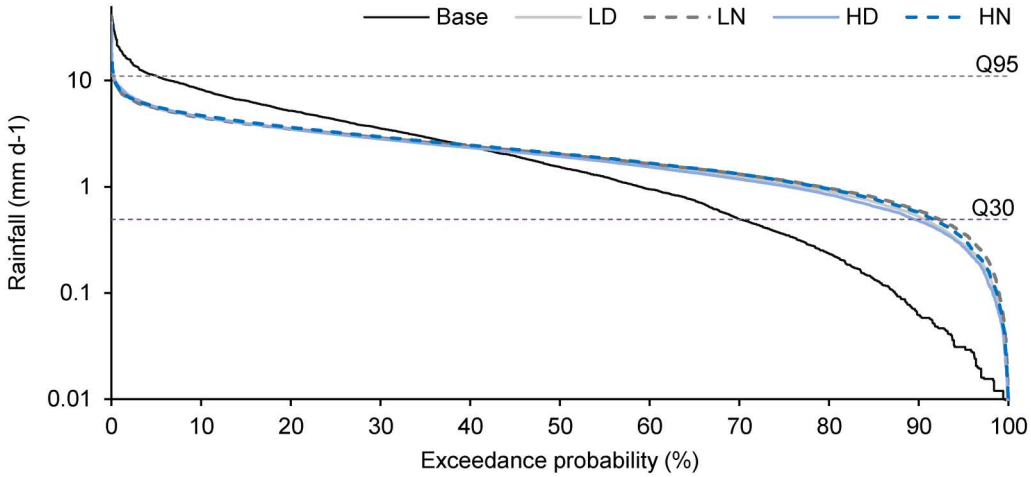

Figure 3. Rainfall duration curve for the base period (2010-2019) and KNMI'23 climate scenarios (2050). Q30 and Q95 are 30th and 95th quantiles, respectively.

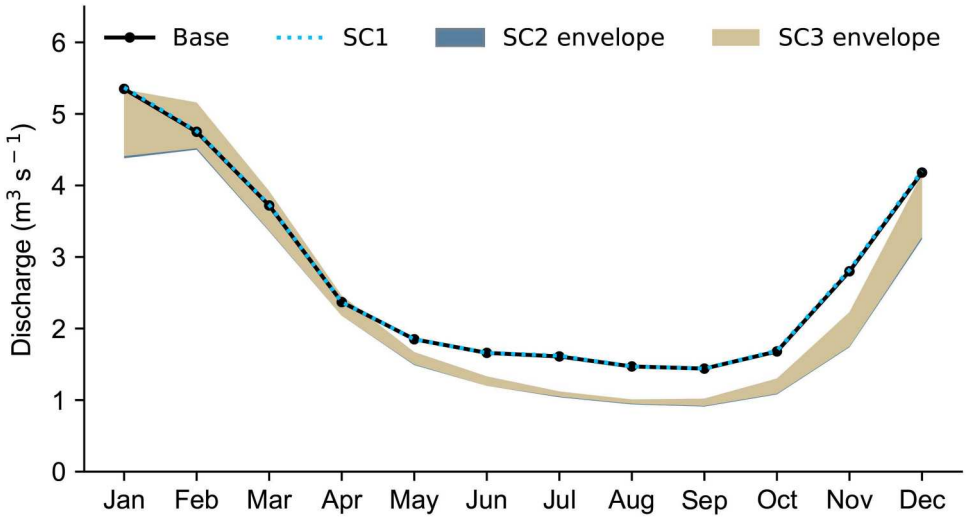

Figure 4. Mean monthly discharge at the catchment outlet under the base, SC1, SC2, and SC3 scenarios. For SC2 and SC3, the envelope represents the range between the highest and lowest values under LD, LN, HD, and HN climate scenarios.

during autumn, with only a 0.7% rise, while the minimum increase is during the spring months, equal to 0.2% (Table 4). This may be attributed to the projected increase in built-up areas in the future, where the expansion of the built-up area (1.7%) dominates the forest and semi-natural (FSN) area expansion (0.4%). This LULC change reduced actual evapotranspiration (AET), leading to more water being retained in the soil and subsequently contributed to increased subsurface flow to river by 0.3–1.1%, with the maximum rise observed in autumn.

The AET is reduced on the catchment scale by – 0.2%, – 0.3%, and – 0.3% in the spring, summer, and autumn respectively, which may be due to a decrease in transpiration from areas that have been converted to built-up areas. On the local scale (Figure 5), considering only the areas where LULC change is projected to occur, the changes in AET range from – 30–22%. Specifically, areas converted to built-up from agriculture and those transitioning from CCP to LPA exhibited a wide range of percentage changes during the spring and summer. In the summer, AET decreased by up to – 20% for most of the areas that transitioned to built-up and LPA, while it increased by up to 5% for the areas that transitioned to FSN (Figure 6). During the winter season, AET for LPA started to increase, reached its maximum in the spring, and decreased in the summer and autumn. This pattern is likely attributed to the sowing and harvesting season for crops in that area. In spring, crops are in full growth, resulting in the maximum AET. In autumn, all transitioned areas experienced a decrease in AET ranging from 0 to – 20%, while the transitioned area to FSN class showed minimal change. In winter, all transitioned cells experience an increase in AET, with a maximum of 8% in places that have been transitioned to built-up areas.

Considering catchment average values, the recharge to groundwater was increased during the summer, autumn, and winter (1.7%, 0.7%, and 0.1%), while experiencing a slight reduction in the spring (0.4%). However, on a local scale, the change in GWT fluctuated between – 10–10%. The changes were mostly positive in autumn and winter. During the spring and summer, most of the transitioned areas exhibited positive change except for a few areas belonging to the built-up area and LPA classes, where the change was negative. Overall, the change in GWT is minimal compared to the variations in AET and SM.

In spring, SM values varied from – 8–10%, with most transitioned areas exhibiting negative changes. During the summer, SM in areas that transitioned to LPA and FSN remained minimal while most of the built-up area exhibited

Table 4. Relative change in water balance component calculated as percentage change with reference to the base period for design scenarios SC1, SC2, and SC3.

	Scenario SC1					Scenario SC2				Scenario SC3			
	Spr	Sum	Aut	Win		Spr	Sum	Aut	Win	Spr	Sum	Aut	Win
Δ AET (%)	−0.2	−0.3	−0.3	0.1	LD	13.5	15.7	12.3	14.2	13.4	15.4	12.2	14.2
					LN	13.3	16.5	12.4	15.2	13.2	16.2	12.3	15.2
					HD	13	15.7	13	14.6	12.8	15.3	12.7	14.6
					HN	11.9	16.6	11.2	13.8	11.8	16.3	11	13.8
Δ Base + drain flow to river (%)	0.3	0.7	1.1	0.5	LD	−11.7	−44.4	−42.2	−12.6	−11.4	−43.9	−41.6	−12
					LN	−7	−40.1	−32.2	−4.8	−6.7	−39.6	−31.6	−4.3
					HD	−4	−44.5	−47.4	−11.3	−3.5	−43.9	−46.7	−10.6
					HN	3.7	−36.6	−29.8	5.2	4	−36.1	−29.2	5.8
Δ Recharge (%)	−0.4	1.7	0.7	0.1	LD	−31.8	−121.1	−21.9	−3	−32	−120	−21.2	−2.7
					LN	−25.4	−107.6	−12.7	−0.4	−25.6	−106.7	−11.9	−0.1
					HD	−20.5	−139.5	−28.3	2.4	−20.6	−138.4	−27.4	2.7
					HN	−11	−116.1	−8.4	7.8	−11.1	−115.2	−7.7	8.1
Δ Discharge (%)	0.2	0.3	0.7	0.3	LD	−11.4	−32.2	−33.3	−14.4	−11.1	−31.9	−32.9	−13.9
					LN	−7.7	−29.5	−25.7	−7.2	−7.5	−29.2	−25.3	−6.8
					HD	−4.9	−32.3	−37	−13	−4.6	−32	−36.6	−12.4
					HN	1.1	−27.3	−23.8	2	1.4	−27	−23.4	2.4

Acronyms used in the table: Δ = relative change, Spr = spring, Sum = summer, Aut = autumn, Win = winter, – sign indicates decrease in value.

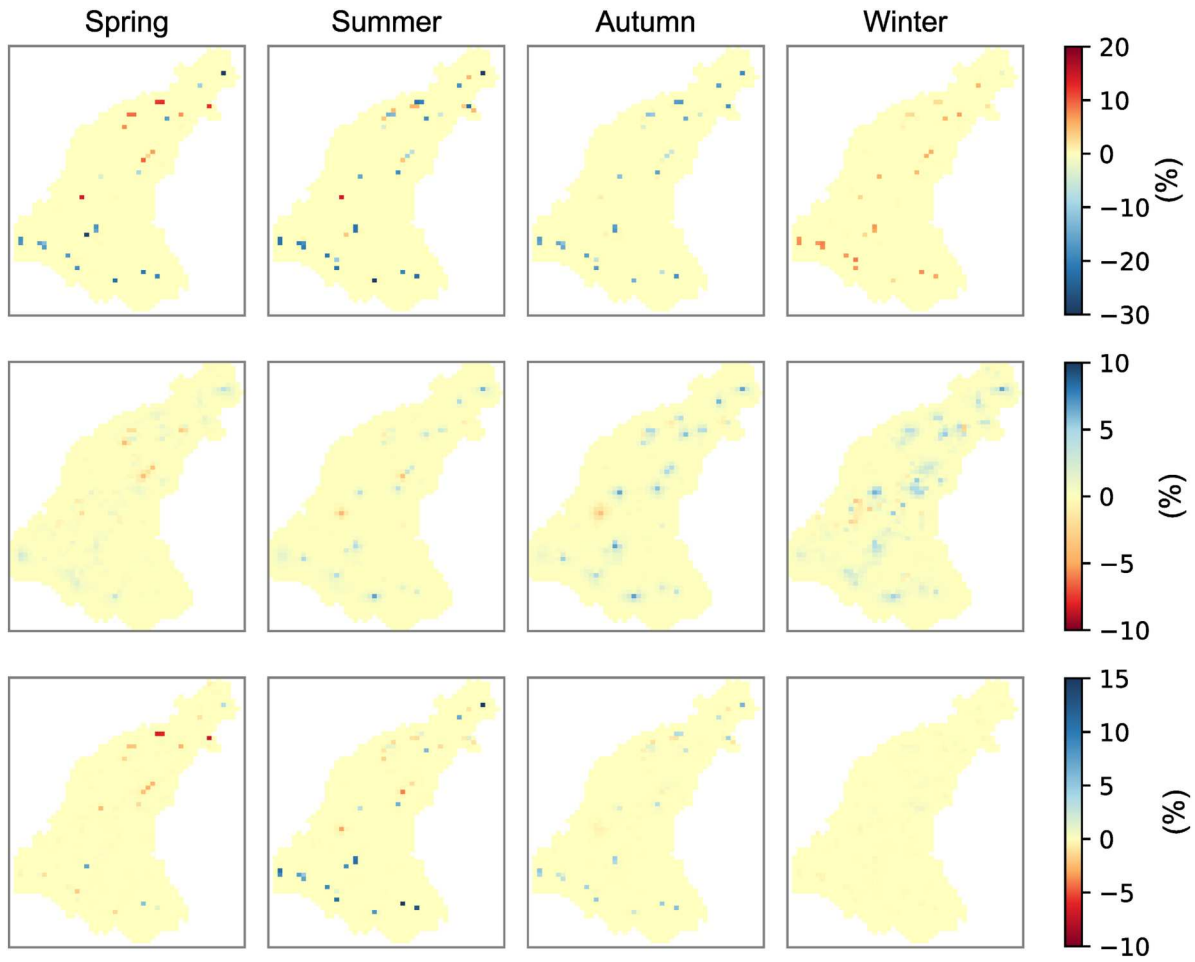

Figure 5. Relative change in simulated AET (upper), GWT (middle), and SM (lower) under base period and SC1 scenarios, calculated as a percentage on the seasonal basis.

changes, ranging from – 5–18%. In autumn, apart from areas that transitioned to FSN, where SM decreased by up to – 2%, other areas exhibited positive changes of up to 7%. During the winter months, SM remained almost unchanged, although AET and GWT exhibited positive changes. This could be due to the presence of already high-water content in the soil layer during winter, keeping SM relatively unaffected.

The percentage differences in AET, SM, and GWT under future LULC (2046), relative to the base period, were plotted against each other to analyse their relationships and sensitivities in different seasons and during transitions of the area from one LULC class to another. GWT changes exhibit minimal sensitivity to variations in SM and AET in spring and summer where wide changes in SM and AET correspond to minor GWT variations. In autumn, the relations between changes in SM and AET become relatively more sensitive to GWT changes, with an increase in SM by up to 7% and a decrease in AET by up to – 20% resulting in a change of GWT by a maximum of 10%. However, during winter months, even with no change in SM and an increase in AET ranging from 0 to 8%, the GWT across transitioned areas increased up to a maximum of 8%. This increase may be attributed to the slower subsurface hydrological flows compared to the topsoil and surface processes (Yang *et al.* 2020; Leong and Yokoo 2022). Another contributing factor could be the higher saturation of the soil during the winter, where excess rainfall directly contributes to groundwater storage (Van Huijgevoort *et al.* 2020).

The relationship between AET and SM is comparatively more responsive. The maximum positive change in SM (up to 18%) is observed in the summer, corresponding to a change in AET (up to – 22%) for areas that transitioned from agriculture to built-up areas. For areas transitioning into forest and semi-natural areas or LPA, the change remains minimal. In autumn, the decrease in AET (up to 20%) causes an increase of up to 7% in SM. Whereas, in winter, even with an increase in AET (up to 10%), SM remains mostly unchanged.

The relationship between the variables is non-linear and varies depending on the seasons and the transitioned class of LULC. Changes in areas transitioning to FSN remained minimal. Areas transitioning into LPA experienced an increase in AET during spring, causing a decrease in SM. During summer, AET decreased in these cells, leading to an increase in SM, and the same process continued in autumn. In winter, they reached higher saturation levels, and SM remained unaffected despite an increase in AET. Whereas, for areas transitioning to the built-up areas from agriculture, the trend remained random during spring and summer, but they followed a similar trend as LPA during autumn and winter.

3.4.2. Scenario SC2, under future climate change

In scenario SC2, the model was simulated using climate projections data for the horizon 2050 (2036-2065), together with the LULC map of the base period, to assess the individual impact of climate change on the catchment's hydrology.

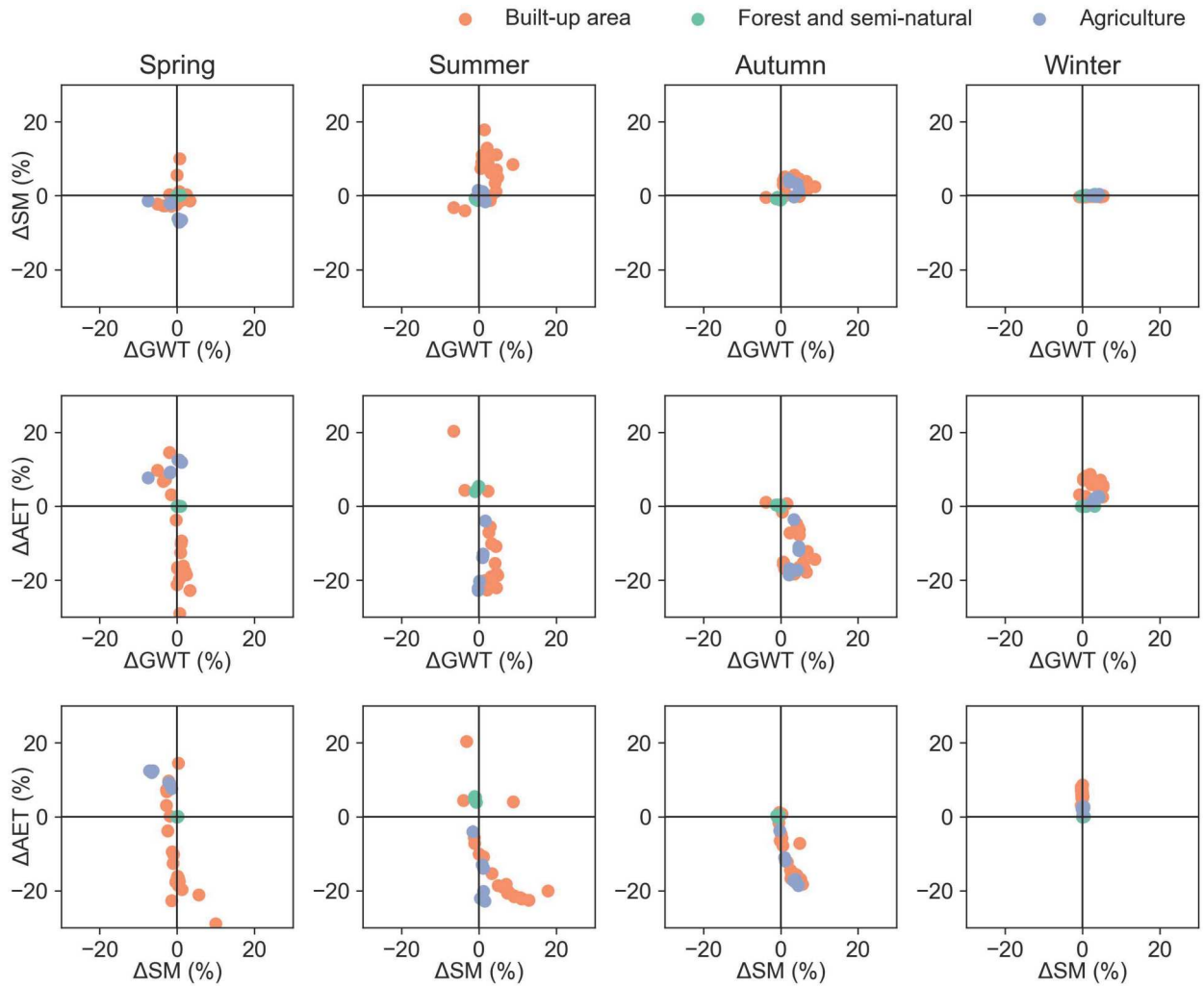

Figure 6. The relationship between the relative change in AET, SM, and GWT on a seasonal basis under the base period and scenario SC1, focusing only on pixels where the LULC is projected to change in the year 2046. Orange represents map pixels transitioning from agriculture to 'Built-up area', green represents pixels transitioning from agriculture to 'Forest and semi-natural (FSN) class', while blue represents pixels projected to change from a 'Complex cultivation pattern (CCP)' to 'Lands principally occupied by agriculture (LPA)'.

The model results revealed that the discharge at the catchment outlet is projected to decrease in January and from April to December under all climate scenarios considered. The lowest average discharges are projected to be observed in September. However, an exception to this trend is noted in February and March, where an increase in discharge relative to the base model is projected only under the HN scenario (Figure 4). It may be attributed to the increased value of PET under all scenarios.

On a seasonal scale, the discharge is projected to decrease by 27.3–32.2% and 23.8–37% in summer and autumn, respectively. In contrast, it ranges between – 11.4–1.1% and – 14.4–2% in spring and winter, respectively (Table 4). This reduction in discharge is likely attributed to a change in catchment average AET which is projected to increase under all climate scenarios by 11.9–13.5%, 15.7–16.5%, 11.2–13%, and 13.8–15.2% in spring, summer, autumn, and winter, respectively. The values across different areas exhibit variation, with certain regions projecting an increase in AET up to 30%, particularly during summer and autumn under LN and HN scenarios (Figure 7). Notably, these areas are characterised by LULC class built-up area and LPA. Conversely, during winter, the change in AET from built-up areas and LPA is less pronounced, with dominance shifting towards LULC classes FSN and CCP.

The maximum change in SM is projected during summer under climate change scenarios LD and HD, where certain areas belonging to classes FSN and CCP show a reduction of up to – 38% and – 40% (Figure 8). Meanwhile, under LN and HN scenarios, SM across the region ranges from – 35–5%. Positive changes are observed only in a small region, possibly attributed to a comparatively lesser increase in AET over those regions. In autumn, SM exhibited both positive and negative changes in the catchment. Under scenarios LD and HD, most areas show negative changes, while the trend reversed under scenarios LN and HN. During winter and spring, the catchment generally experiences positive changes under all scenarios, except for a small section towards the north side of the catchment where changes are negative. Although the trend across different LULC classes appears random, no direct correlation with specific LULC classes influencing an increase or decrease in SM has been identified. However, the negative change (up to – 40%) exhibited during summer outweighs the positive change (up to 10%) observed during winter. Similarly, the catchment's average recharge to groundwater is projected to decrease by – 107.6 to – 139.5% during summer, whereas in spring (−11 to – 31.8%) and autumn (−8.4 to – 28.3%), the change in relative to base period is comparatively less (Table 4). During winter, an increase is projected by 2.4% and 7.8% under HD and

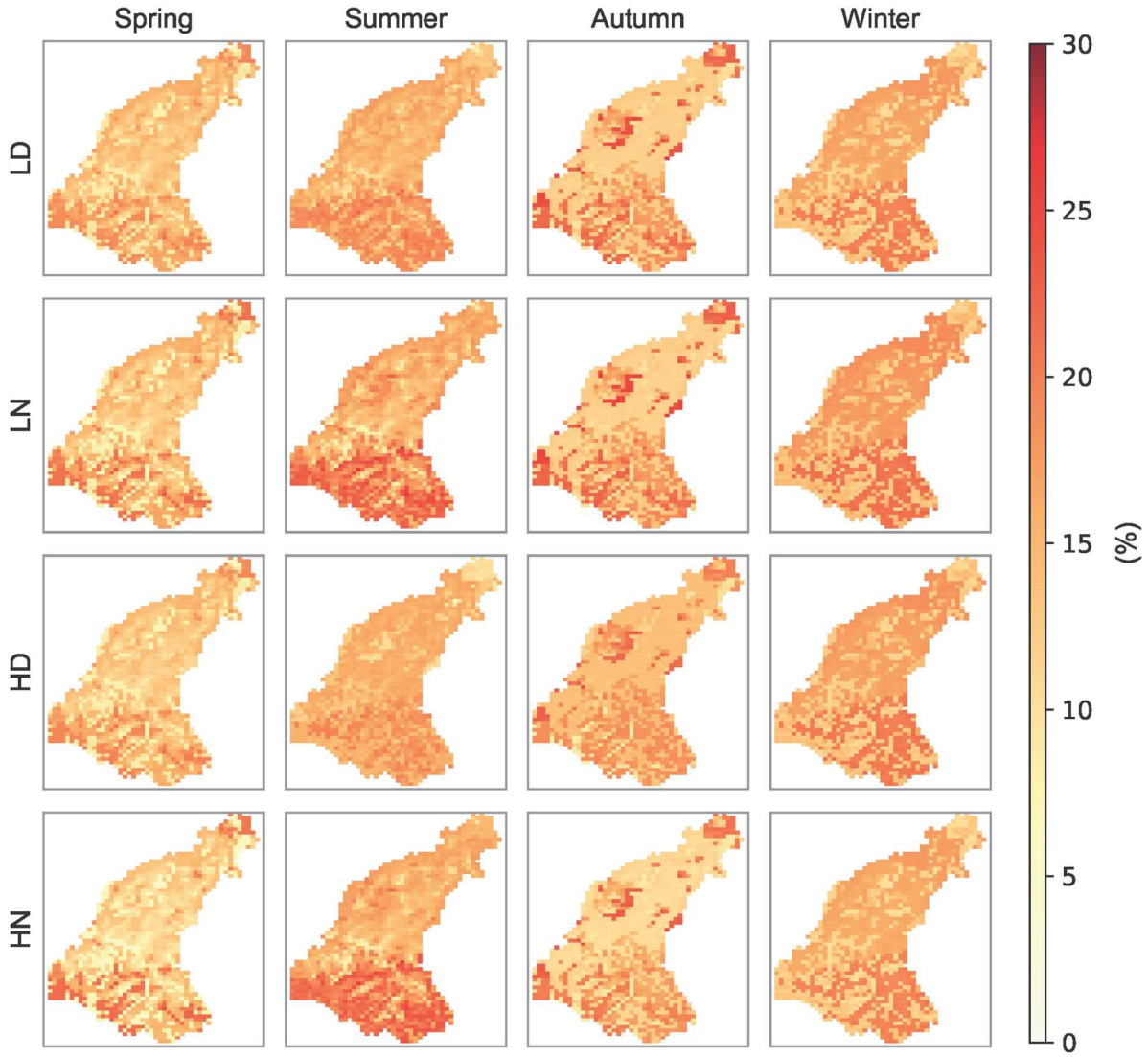

Figure 7. Relative change in simulated AET under the base period and SC2 scenario, calculated as a percentage on the seasonal basis.

HN scenarios, while LD and LN scenarios anticipated a reduction of – 3% and – 0.4%, respectively. These findings highlight the season-specific and scenario-dependent nature of changes in SM. The spatial distribution of percentage change in GWT is shown in Figure 9.

On the local scale, during the summer months, negative changes in GWT are observed across all areas under all scenarios. The maximum negative change, reaching – 50%, is projected under LD and HD scenarios, while it is – 30% under LN and HN scenarios in certain areas having LULC class as agricultural. Moving to autumn, some areas exhibit a GWT increase of 25%, but the major portion of the catchment is likely to have negative changes. Notably, in the central area of the catchment, GWT is projected to decrease by a maximum of – 60% and – 75% under LD and HD scenarios, respectively. Even during winter, changes in the catchment are not spatially uniform, with positive changes observed in the central portion and negative changes in the southern and northern areas of the catchment. A similar trend is observed in spring, though the magnitude of change is comparatively less than in winter.

It is worth noting that across all scenarios and seasons, negative changes in GWT are consistently observed in the area near the outlet of the catchment (north part). The general groundwater flow in the catchment is from southeast to northwest. Due to a lower water table in the middle and upper portions of the catchment, groundwater flow towards the outlet might be comparatively less, impacting the area near the outlet across all seasons.

As discussed in Section 3.2, despite an increase in autumn rainfall, the discharge at the catchment outlet, subsurface flows, recharge, and GWT at most locations exhibited a negative change. Even the SM for the topsoil layer did not show a spatially consistent positive change across the catchment. This phenomenon may be attributed to additional summer stress generated in the catchment due to low rainfall and higher AET. The additional rainfall, compared to the base period, occurring in autumn is consumed to overcome the prevailing summer drawdowns in GWT and soil water content. On the other hand, in spring, the projected increase in rainfall is comparatively less than in autumn, but the discharge at the outlet, along with other variables, exhibited a more positive change than in autumn. This may be because in winter, the GWT and water content in the soil are relatively high, and even a comparatively smaller increase in rainfall contributes more prominently to different hydrological components. This aligns with the findings of Assouline *et al.* (2024), Alam *et al.* (2024) and Ran *et al.* (2022), who highlighted the influence of antecedent conditions on flow generation.

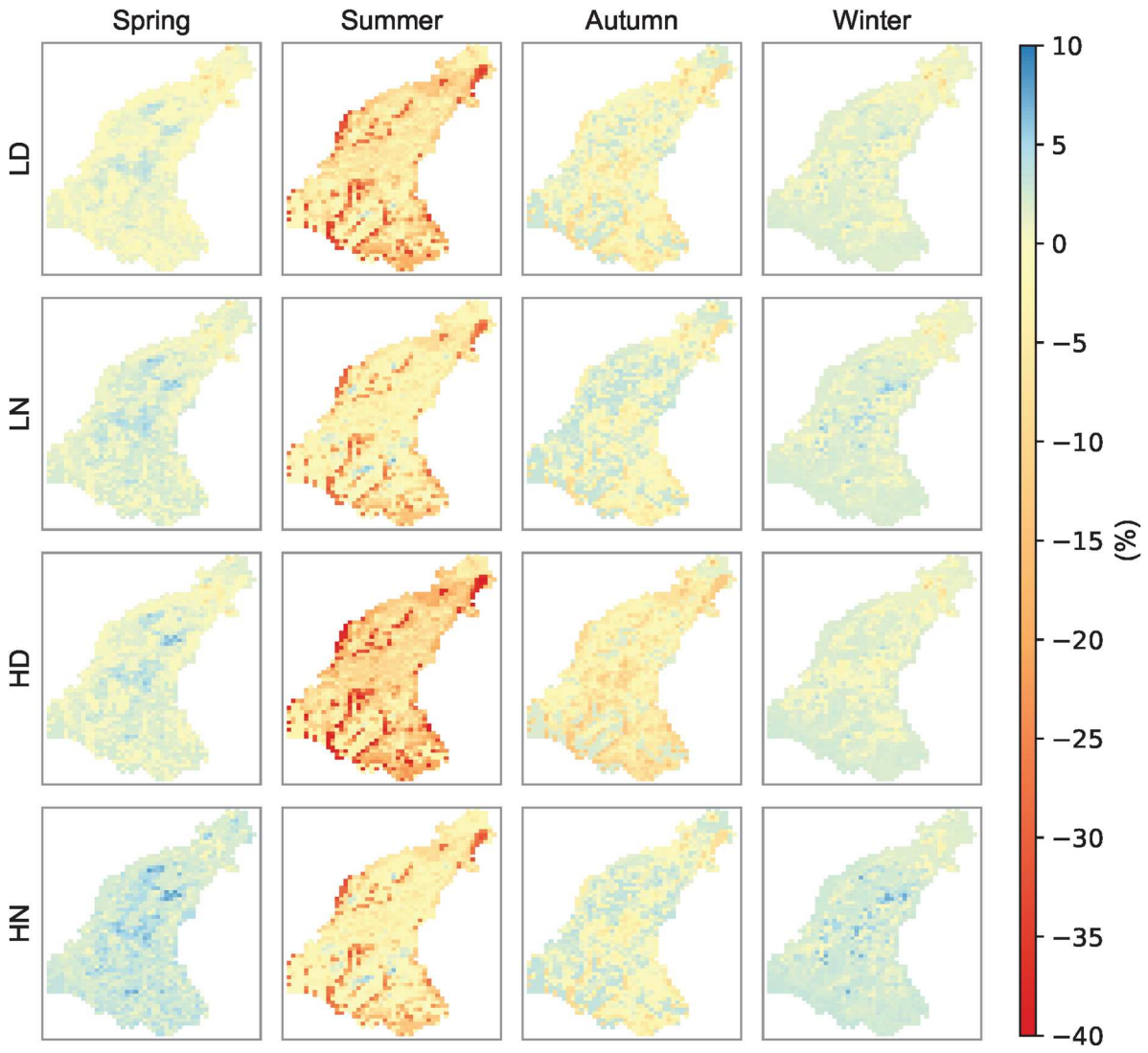

Figure 8. Relative change in simulated SM under the base period and SC2 scenario, calculated as a percentage on the seasonal basis.

3.4.3. Scenario SC3, under future climate and LULC change

In scenario SC3, the model was simulated with climate projections referred to the horizon 2050 (2036-2065), together with the generated future LULC to assess the combined effects on the catchment's hydrology. Notably, the discharge at the catchment outlet across different months under scenario SC3 closely resembles that of scenario SC2, where only climate change was considered (Figure 4). The maximum increase in discharge, compared to scenario SC2, is projected to be 0.5% in winter and 0.3% in summer. This modest change may be attributed to the projected expansion of built-up areas in the future, where the development of the built-up area (1.7%) dominates over FSN area expansion (0.4%). A similar trend was observed in scenario SC1, though the comparative increase in discharge in scenario SC3 is less than that observed in SC1. Likewise, the subsurface flow to the river is projected to increase under the combined effect of climate change and future LULC changes, but the increase in the catchment average is minimal (Table 4).

The situation with AET mirrors the discharge trends. When considering catchment average values, AET is projected to decrease by 0.3–0.4% compared to the individual effect of climate change in the summers, with no projected change in winter. However, to assess changes at the local scale, the spatially distributed relative change in AET compared to the base period was calculated (Figure 10), and found that AET under scenario SC3 is almost identical to scenario SC2, except for a few locations where the relative change in AET has altered. To identify the exact locations where the change has happened under scenario SC3, the differences in percentage changes under scenarios SC2 and SC3 relative to the base model were computed and are represented in Figure S5 of the supplemental material. In spring, summer, and autumn, significant changes in AET are observed over areas that are projected to undergo LULC transition. For example, in summer, compared to scenario SC2, AET is projected to be less by up to 30% in areas transitioning from agriculture to built-up, while it will be more by up to 5% in areas transitioning to FSN from agriculture. In spring and autumn, the differences are comparatively less, and there is no change in winter.

The spatial distribution of SM under scenario SC3 is represented in Figure 11. Similar to AET, the relative change in SM compared to the base period under the combined effect of climate change and future LULC is within the same range as that of the individual effect of climate change, with only a few areas exhibiting notable differences as presented in Figure S6 of the supplemental material. A noteworthy observation is the increased number of areas showing positive changes in summers under the combined effect of climate change and future LULC. These new areas with positive

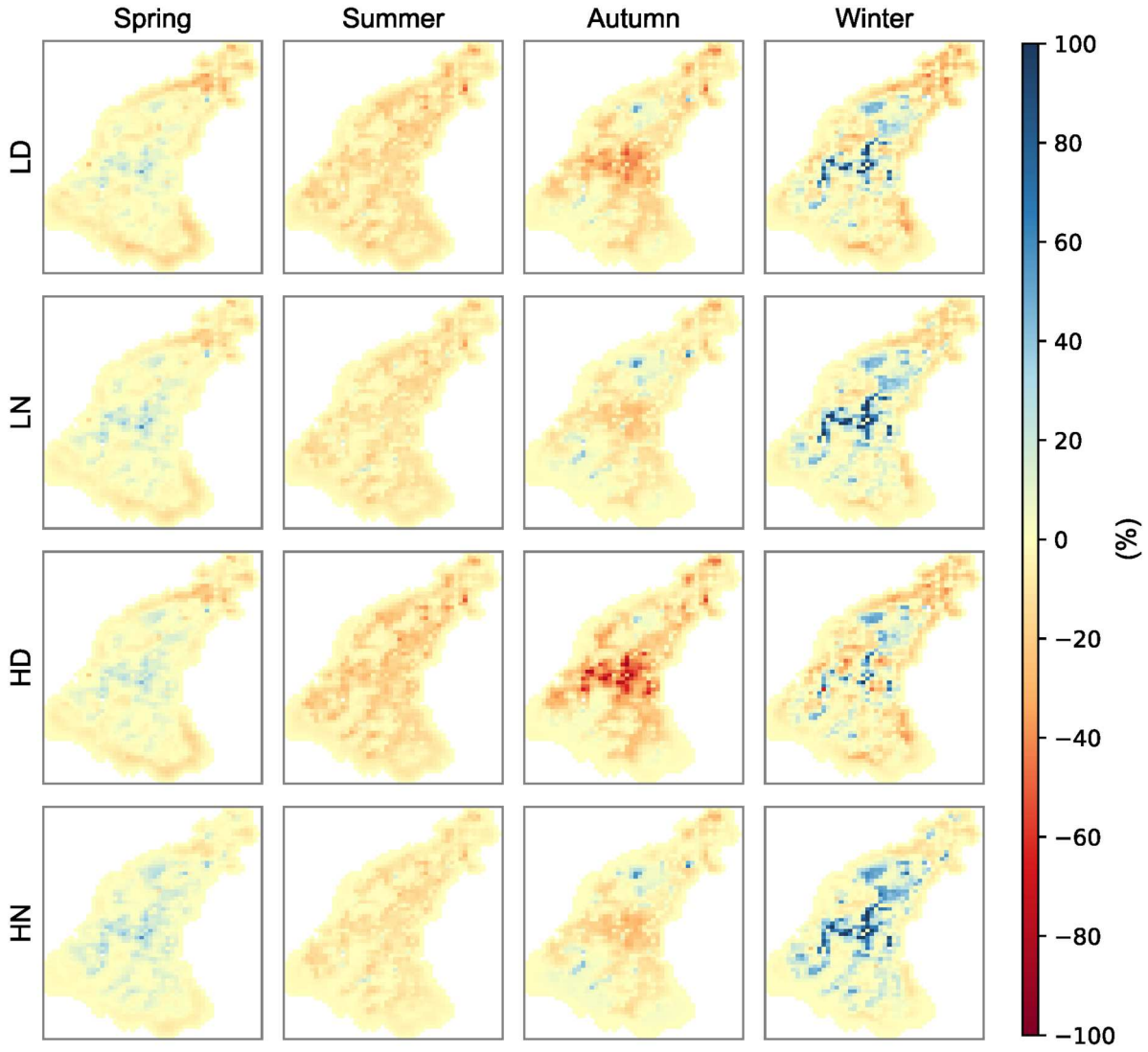

Figure 9. Relative change in simulated GWT under the base period and SC2 scenario, calculated as a percentage on the seasonal basis.

changes in summer are predominantly those that are projected to undergo a transition from agriculture to built-up areas in the future LULC map. The maximum projected change in these areas is reaching up to a maximum of 30%. Conversely, in areas transitioning to FSN, the change is reduced, up to a maximum of – 4%. During the winter, there is no change in simulated SM under scenarios SC2 and SC3.

Considering the catchment average values, recharge to groundwater is projected to decrease under scenario SC3, aligning with the trend observed in scenario SC2. However, under scenario SC3, the recharge values differ by a maximum of 0.6% and 0.7% in summer and winter, respectively, under the HD scenario of climate change. In other seasons and climate scenarios, the differences are even less (Table 4). Similar to AET and SM, the variations in GWT at the local scale in transitioning areas are more pronounced than changes in catchment averages. The spatial distribution of GWT and the differences in percentage changes under scenarios SC2 and SC3 relative to the base model are illustrated in Figure 12 and Figure S7, respectively. The seasonal and spatial trends under scenario SC3 are consistent with those of SC2, but in a few of the areas, the values of percentage change have shifted within the range of – 5–15%. For instance, during winter, in areas transitioning to the built-up, the GWT is projected to further rise by 15% compared to the relative change projected under scenario SC2. These changes are particularly noticeable in autumn and winter compared to spring and summer.

It is crucial to note that the changes in GWT are not limited to the areas that are projected to undergo future LULC transitions, but changes in neighbouring areas are also observed. In contrast to GWT, the influence on neighbouring areas has not been observed for SM. This distinction may be attributed to the modelling constraints in MIKE SHE, where the exchange of flow in the unsaturated zone is primarily permitted in the vertical direction, limiting the simulation of soil moisture exchanges in the horizontal direction.

The overall findings suggest that hydrological components are more influenced by climate change alone (SC2) than by the LULC change scenario (SC1). Furthermore, on the catchment scale, the combined effect of climate and LULC changes (SC3) does not significantly differ from the individual effect of climate change (SC2). These results align with studies conducted by Getachew *et al.* (2021) and Yan *et al.* (2019), both of which identified hydrological components as more sensitive to climate change on both seasonal and annual scales. In the combined effect of LULC and climate change (SC3), the impact of climate change appears

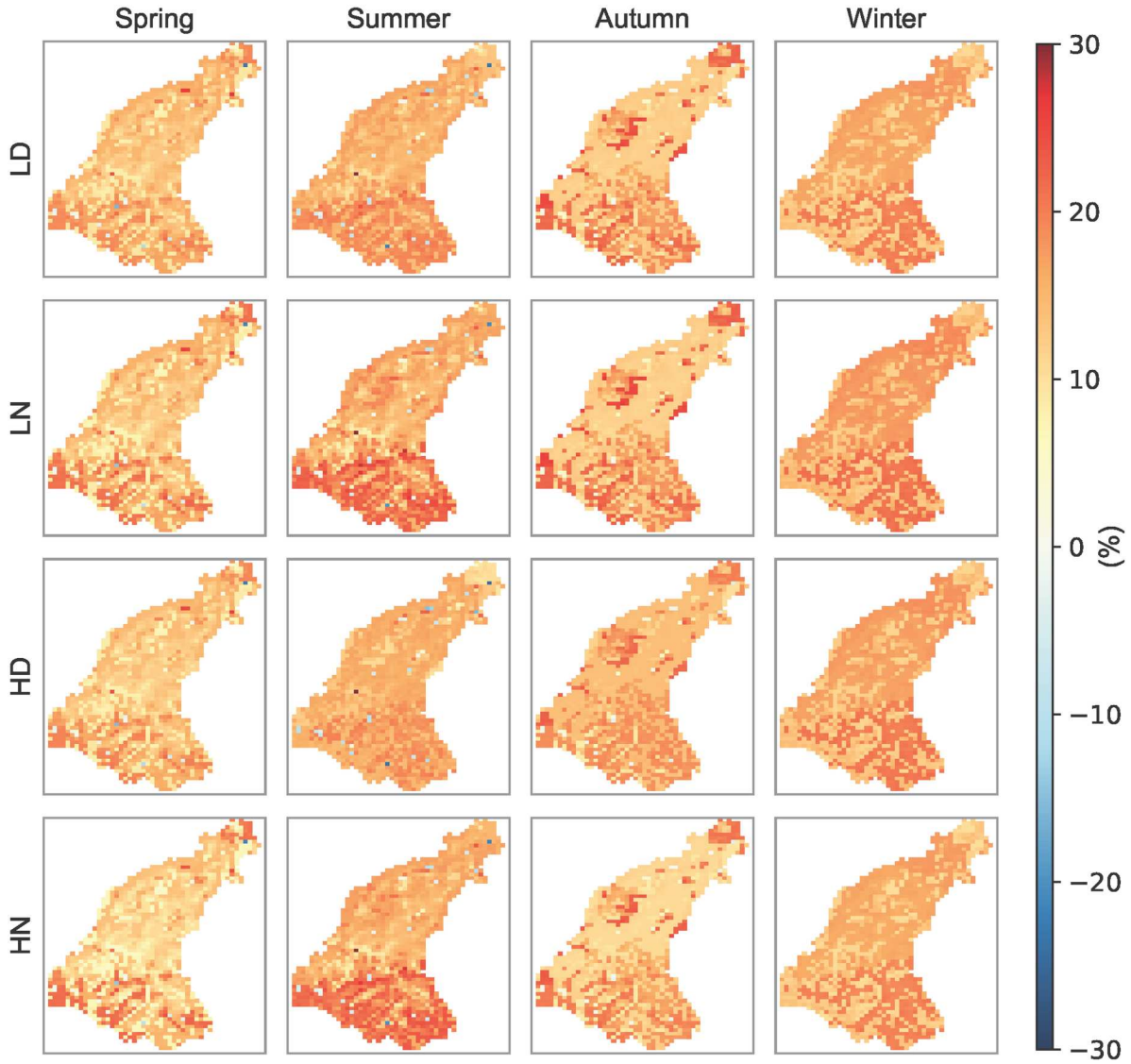

Figure 10. Relative change in simulated AET under the base period and SC3 scenario, calculated as a percentage on the seasonal basis.

to be somewhat dampened by the effects of LULC change. Similar findings have been reported by Tirupathi and Shashidhar (2020), although in this study, the offsetting influence of LULC change is very minimal, accounting for less than 1% on the catchment scale.

However, in contrast to this, the impact of LULC changes is more pronounced at the local scale, particularly in areas projected to transition from one LULC class to another. The incorporation of LULC changes, alongside climate change, can significantly influence the relative changes in GWT, SM, and AET on the local scale, with variations referred to scenario SC2 ranging from approximately – 6–15%, – 9–27%, and – 30–10%, respectively, depending upon the specific change in LULC class and season.

This nuanced spatial distribution of changes in hydrological variables underscores the role of LULC changes in conjunction with climate impacts, highlighting specific areas undergoing transitions as significant contributors to the observed variations in hydrological dynamics. Understanding these localised effects is crucial for effective water resource management and climate change adaptation strategies within the catchment. These findings underscore the importance of considering both climate change and future LULC changes in assessing the hydrological response of the catchment particularly if the focus is on local scales.

4. Conclusions

This research assesses the response of surface (AET, discharge) and subsurface (recharge, GWT, SM, and lateral flow) hydrological components to the separate and combined future changes in climate and LULC at a catchment and local scales for the Aa of Weerijs catchment. To conduct the research, a physically based fully distributed hydrological model was set up for the study area, using MIKE SHE and MIKE 11 modelling tools. The ANN-CA technique was employed to simulate future LULC changes using the MOLUSCE plugin of QGIS. Validation of the LULC prediction model demonstrated satisfactory accuracy, with kappa coefficients ranging from 0.94–0.97 and a percentage correctness of 95.7%. The analysis of historical (2018) and simulated LULC for the year 2046 identified a 1.7% expansion in built-up and a 0.4% increase in FSN class.

For meteorological projections under climate change, the data was acquired from KNMI'23 climate scenarios for the 2050 horizon (2036-2065). The time series of catchment average rainfall and PET were compared with data from

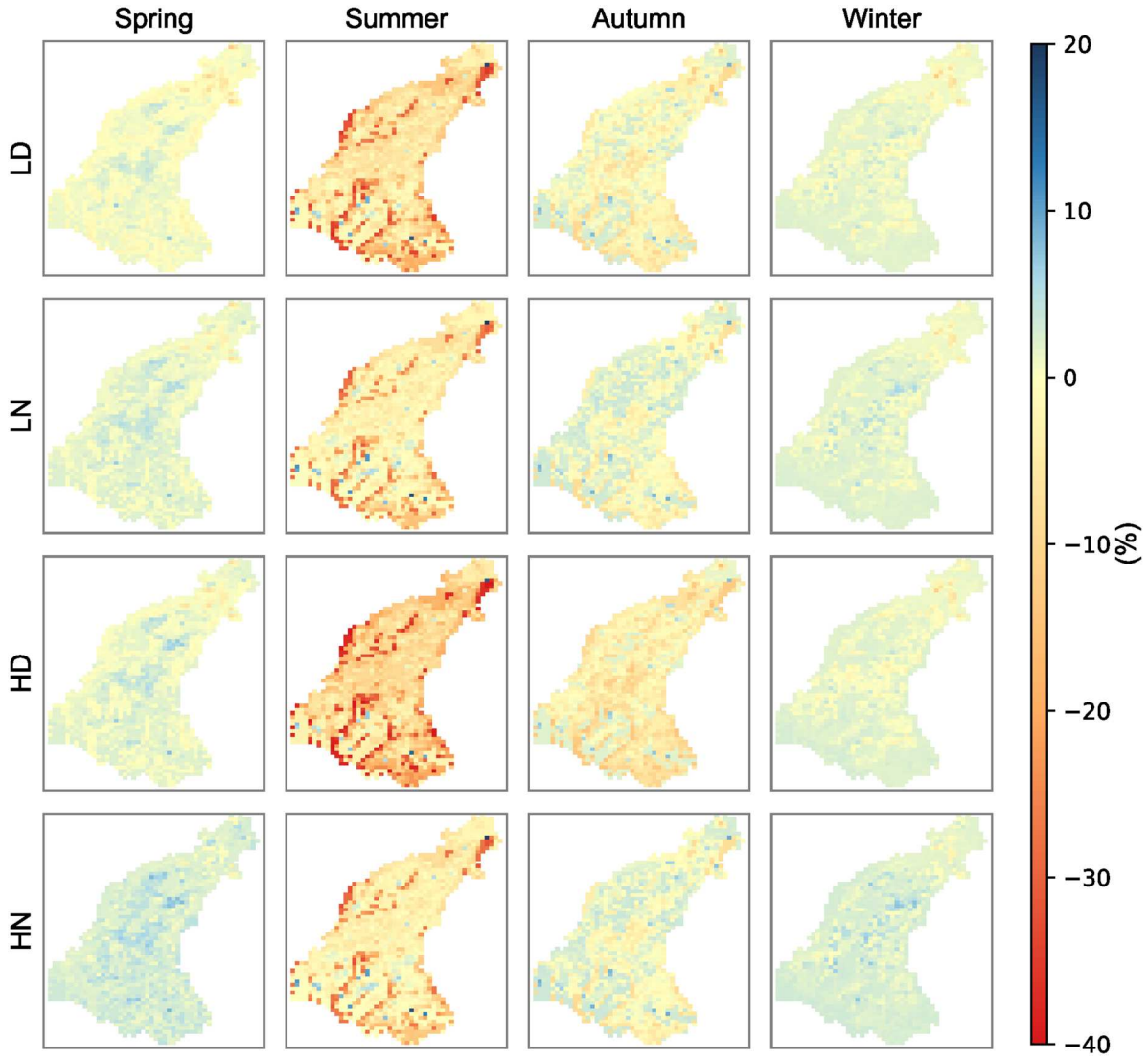

Figure 11. Relative change in simulated SM under the base period and SC3 scenario, calculated as a percentage on the seasonal basis.

the historical (base) period and the results suggested an overall increase in PET across all scenarios, with varying patterns of rainfall changes. The increase in PET is more pronounced than the changes in rainfall. The summer showed a tendency for decreased rainfall coupled with a substantial increase in PET, highlighting potential water stress during critical periods.

The simulated results only with future LULC changes revealed that the impacts on catchment hydrology are minimal. The expansion of built-up areas contributes to a modest increase in discharge and subsurface flow, while changes in AET, GWT, and SM show localised variations. Under the individual impacts of climate change, the changes in hydrological variables are comparatively more pronounced. Considering both future LULC and climate change demonstrated that while hydrological variables were more sensitive to climate change alone, the combined effects did not significantly differ from the individual impact of climate change on the catchment scale. However, at the local scale, especially in areas undergoing LULC transitions, the combined effects exhibited significant variations in hydrological variables.

To address the specific research question raised, we concluded that for the lowland catchment with a size of 346 km^2 and projected increase in built-up area by 1.7% and FSN by 0.4%, the impact of including future LULC data in addition to climate change projections, is not significant at the catchment scale, as it accounts for very minimal changes in hydrological variables (>1%). However, at the local scales, it can significantly influence the relative changes in GWT, SM, and AET with variations ranging from approximately – 6–15%, – 9–27%, and – 30–10% respectively, depending on the specific change in LULC class and season. The spatial distribution of changes in AET, SM, and GWT emphasises the importance of considering localised impacts for effective water resource management. The study underscores the importance of considering both climate and land use dynamics for a comprehensive understanding of hydrological changes in the face of future challenges.

While this study has provided valuable insights, there are certain limitations that warrant consideration. Firstly, the future LULC scenario adopted here is based on a business-as-usual approach. A more nuanced understanding could be achieved by formulating different scenarios for future LULC, incorporating constraints on LULC class expansion, and considering local landscape policies, municipal priorities, or broader European-level policies. Such considerations could enhance the refinement of future LULC projections.

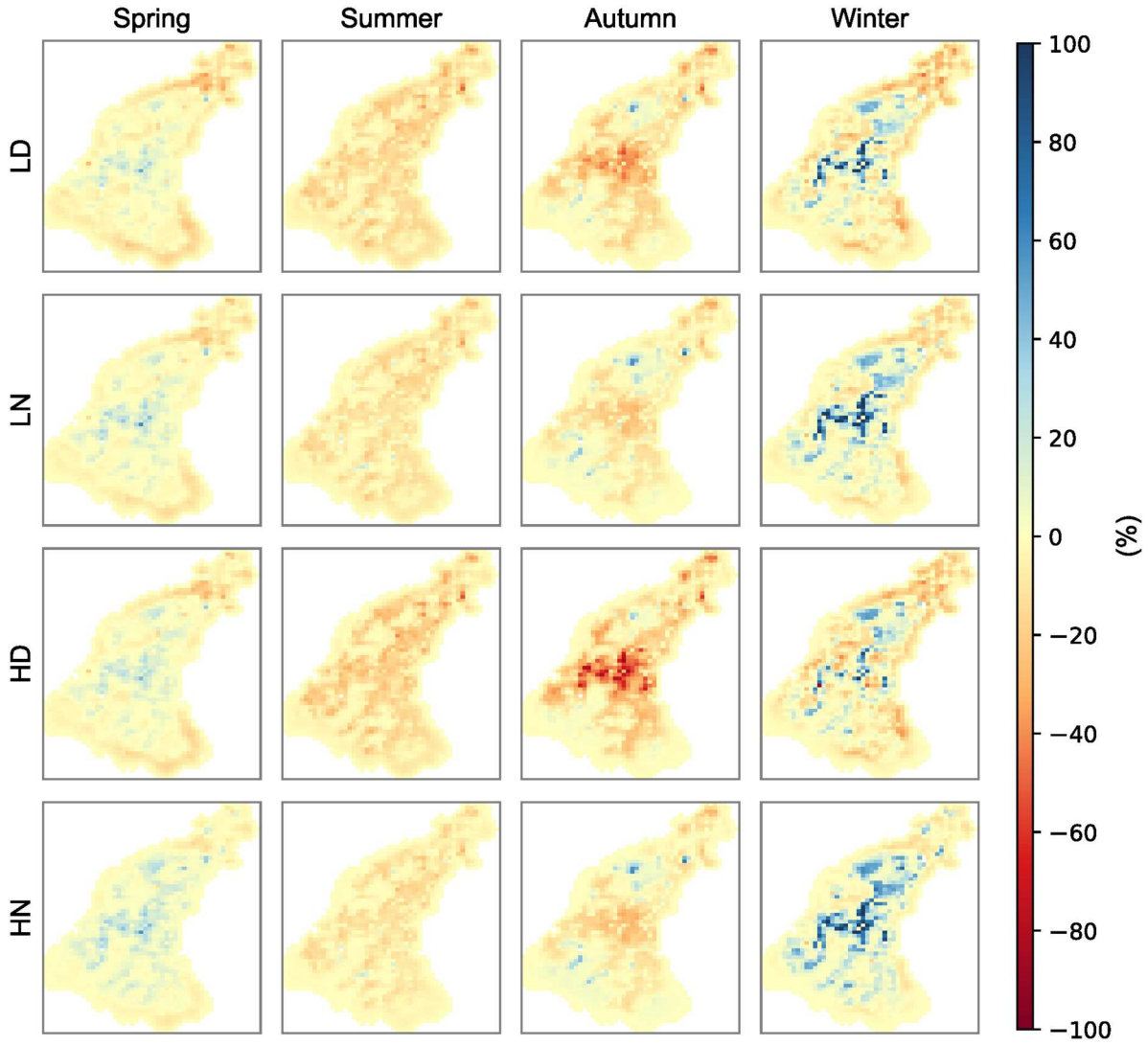

Figure 12. Relative change in simulated GWT under the base period and SC3 scenario, calculated as a percentage on the seasonal basis.

Secondly, the study focused only on rainfall, PET, and LULC under future changes. Global warming may trigger additional factors, such as groundwater abstraction or direct water abstraction from rivers, which could impact discharge and GWT. Additionally, changes in groundwater boundary conditions, not accounted for in this study's future scenarios, could further influence hydrological dynamics. Therefore, future research activities could address these limitations by incorporating these additional factors. The effect of these factors might not be significant alone but studying the coupled effects of various drivers would provide a more comprehensive understanding of future hydrological dynamics. Such insights could offer more detailed information to policy-makers, aiding in the development of informed and robust strategies for sustainable water resource management.

Acknowledgments

We thank the Water Board Brabantse Delta, Breda, the Netherlands, for data provision and the Danish Hydraulic Institute, Denmark for providing access to the MIKE ZERO modelling package.

Disclosure statement

No potential conflict of interest was reported by the author(s).

Funding

The research presented here is supported by the European Union's Horizon 2020 research and innovation programme 'EIFFEL project' [Grant Number: 101003518].

Data availability statement

The used data in modelling along with sources are presented in Table 1. The links for downloading the data can be found in the references corresponding to each data type. For the simulation of future LULC map, the historic LULC data was obtained from Corine Land Cover (CLMS n.d.-b). The elevation data was obtained from European Digital Elevation Model (EU-DEM v1.1, CLMS, n.d.-a). The road network was extracted from OpenStreetMap (OSM) using OSMDownloader plugin in QGIS which is available at https://plugins.qgis.org/plugins/OSMDownloader/. Further, the data that support the findings of this study are available from the corresponding author upon reasonable request.

Notes on contributors

Muhammad Haris Ali is a PhD researcher at the IHE Delft Institute for Water Education and Delft University of Technology, Netherlands. He holds an MSc in Hydroinformatics from IHE Delft and has a background in Civil Engineering. Haris specializes in hydrological and hydraulic modelling, surface-subsurface hydrological interactions, machine learning, land-use and climate change analysis, nature-based solutions, and operational water management.

Dr *Claudia Bertini* is a lecturer and researcher in the Hydroinformatics group at IHE Delft Institute for Water Education in Delft, the Netherlands. She holds an MSc degree in Civil Hydraulic Engineering and a PhD degree in Environmental and Hydraulics Engineering from Sapienza University of Rome, Italy. Her background is in hydrology, with experience in rainfall data analysis, rainfall extreme events, remote sensing, hydrological modelling, and Machine Learning for hydrological forecasting.

Professor *Ioana Popescu* works in the field of Hydroinformatics, currently serving as a zero appointed Professor of Hydroinformatics at TU Delft and actively contributing to the mission and vision of IHE Delft in The Netherlands. Her research area focusses in integrating computational methods for water resources into decision support systems. Her work particularly focuses on river systems and lakes, with applications in flood modelling for management and water resources management.

Dr *Andreja Jonoski* received his BSc degree in civil engineering from the University of St. Cyril and Methodius - Skopje, in 1988. Until 1994, he worked at the Civil Engineering Institute, Macedonia, in the Geotechnics division, first as a groundwater hydrologist and later as head of the division. He received the MSc degree in groundwater hydrology and the Ph.D. degree in Hydroinformatics from IHE Delft, Delft, the Netherlands, in 1996 and in 2002, respectively. He has worked as a staff member of the Hydroinformatics Chair Group, where he currently serves as an Associate Professor of Hydroinformatics. His research interests include modelling of natural and urban water systems, model-based optimization and water-related decision support systems, including web- and mobile-phone applications for participatory and collaborative decision support in the fields of water and the environment.

ORCID

Muhammad Haris Ali http://orcid.org/0009-0001-0240-6851
Claudia Bertini http://orcid.org/0000-0003-3315-1801
Ioana Popescu http://orcid.org/0000-0002-1009-5424
Andreja Jonoski http://orcid.org/0000-0002-0183-4168

References

Adib, M. N. M., *et al.*, 2020. Projected streamflow in the Kurau River Basin of Western Malaysia under future climate scenarios. *Scientific Reports*, 10 (1), 8336.

Alam, S., *et al.*, 2024. The role of antecedent winter soil moisture carryover on spring runoff predictability in snow-influenced Western US catchments. *Journal of Hydrometeorology*, 25 (10), 1561–1575.

Ali, M. H., *et al.*, 2023. Remote sensed and/or global datasets for distributed hydrological modelling: A review. *Remote Sensing*, 15 (6), 1642.

AR6, 2023. IPCC, 2023: Climate change 2023: synthesis report, summary for policymakers. contribution of working groups I, II and III to the sixth assessment report of the intergovernmental panel on climate change. IPCC, Geneva, Switzerland.

Assouline, S., *et al.*, 2024. Runoff generation in a semiarid environment: The role of rainstorm intra-event temporal variability and antecedent soil moisture. *Advances in Water Resources*, 188, 104715.

Ballabio, C., *et al.*, 2019. Mapping LUCAS topsoil chemical properties at European scale using Gaussian process regression. *Geoderma*, 355, 113912.

Ballabio, C., Panagos, P., and Monatanarella, L., 2016. Mapping topsoil physical properties at European scale using the LUCAS database. *Geoderma*, 261, 110–123.

Beers, M., *et al.*, 2018. Water systeem analyse Aa of Weerijs.

Blöschl, G., *et al.*, 2019. Changing climate both increases and decreases European river floods. *Nature*, 573 (7772), 108–111.

Boussinesq, J., 1904. Recherches théoriques sur l'écoulement des nappes d'eau infiltrées dans le sol et sur le débit des sources. *Journal de mathématiques pures et appliquées*, 10, 5–78.

Cannon, A. J., Sobie, S. R., and Murdock, T. Q., 2015. Bias correction of GCM precipitation by quantile mapping: how well do methods preserve changes in quantiles and extremes? *Journal of Climate*, 28 (17), 6938–6959.

Chow, V. T., 1959. *Open-channel hydraulics*. New York: US Army Corps of Engineers, Hydrologic Engineering.

CLMS, n.d.-a. Copernicus land monitoring service Corine EU-digital elevation model [online]. Available from: https://land.copernicus.eu/imagery-in-situ/eu-dem/eu-dem-v1-1-and-derived-products/eu-dem-v1.1?tab=download. [Accessed 27 November 2023].

CLMS, n.d.-b. Copernicus land monitoring service Corine land cover 2018 [online]. Available from: https://land.copernicus.eu/pan-european/corine-land-cover/clc2018 [Accessed 27 November 2023].

de Klein, J. J., and Koelmans, A. A., 2011. Quantifying seasonal export and retention of nutrients in West European lowland rivers at catchment scale. *Hydrological Processes*, 25 (13), 2102–2111.

Feranec, J., *et al.*, 2016. CORINE land cover nomenclature. *European landscape dynamics: CORINE land cover data*; Feranec, J., *et al.*, ed. Boca Raton: CRC Press, 17–25.

Fu, Q., *et al.*, 2019. Effects of land-use change and climate variability on streamflow in the Woken River basin in Northeast China. *River Research and Applications*, 35 (2), 121–132.

Getachew, B., Manjunatha, B., and Bhat, H. G., 2021. Modeling projected impacts of climate and land use/land cover changes on hydrological responses in the Lake Tana Basin, upper Blue Nile River Basin, Ethiopia. *Journal of Hydrology*, 595, 125974.

Ghimire, U., *et al.*, 2021. Climate and land-use change impacts on spatiotemporal variations in groundwater recharge: A case study of the Bangkok Area, Thailand. *Science of the Total Environment*, 792, 148370.

Gunnink, J., *et al.*, 2013. Digital Geological Model (DGM): a 3D raster model of the subsurface of the Netherlands. *Netherlands Journal of Geosciences*, 92 (1), 33–46.

Gurara, M. A., Jilo, N. B., and Tolche, A. D., 2021. Modelling climate change impact on the streamflow in the Upper Wabe Bridge watershed in Wabe Shebele River Basin, Ethiopia. *International Journal of River Basin Management*, 21 (2), 181–193.

Hanifehlou, A., *et al.*, 2022. Sustainable exploitation of groundwater resources considering the effects of climate change and land use to provide adaptation solutions (case study of the Hashtgerd plain). *Acta Geophysica*, 70 (4), 1829–1846.

Hofstra, N., *et al.*, 2008. Comparison of six methods for the interpolation of daily, European climate data. *Journal of Geophysical Research: Atmospheres*, 113 (D21), http://dx.doi.org/10.1029/2008JD010100.

Huq, E., and Abdul-Aziz, O. I., 2021. Climate and land cover change impacts on stormwater runoff in large-scale coastal-urban environments. *Science of the Total Environment*, 778, 146017.

Iqbal, M., *et al.*, 2022. Impacts of climate and land-use changes on hydrological processes of the source region of Yellow River, China. *Sustainability*, 14 (22), 14908.

IWMI, 2019. Innovative Water Solutions for Sustainable Development; IWMI Strategy 2019–2023. Colombo, Sri Lanka.

Jian, S., *et al.*, 2022. The possible incoming runoff under extreme rainfall event in the Fenhe river basin. *Frontiers in Environmental Science*, 10, 812351.

Kafy, A.-A., *et al.*, 2020. Modelling future land use land cover changes and their impacts on land surface temperatures in Rajshahi, Bangladesh. *Remote Sensing Applications: Society and Environment*, 18, 100314.

Kay, A., *et al.*, 2021. Climate change effects on indicators of high and low river flow across Great Britain. *Advances in Water Resources*, 151, 103909.

KNMI, n.d. Koninklijk Nederlands Meteorologisch Instituut (Royal Netherlands Meteorological Institute) [online]. Available from: https://www.knmi.nl/nederland-nu/klimatologie [Accessed 27 November 2023].

Kundu, S., Khare, D., and Mondal, A., 2017. Individual and combined impacts of future climate and land use changes on the water balance. *Ecological Engineering*, 105, 42–57.

Lee, H., *et al.*, 2024. Climate change 2023 synthesis report summary for policymakers. CLIMATE CHANGE 2023 Synthesis Report: Summary for Policymakers.

Leong, C., and Yokoo, Y., 2022. A multiple hydrograph separation technique for identifying hydrological model structures and an interpretation of dominant process controls on flow duration curves. *Hydrological Processes*, 36 (4), e14569.

Liu, X., *et al.*, 2017. A future land use simulation model (FLUS) for simulating multiple land use scenarios by coupling human and natural effects. *Landscape and Urban Planning*, 168, 94–116.

Loliyana, V. D., and Patel, P. L., 2020. A physics based distributed integrated hydrological model in prediction of water balance of a semi-arid catchment in India. *Environmental Modelling and Software*, 127, 104677.

Lyu, Y., *et al*., 2023. Identifying the Impacts of Land Use Landscape Pattern and Climate Changes on Streamflow From Past to Future. Available at SSRN 4388252, 345, 118910.

Ma, L., *et al*., 2016. MIKE SHE modeling of ecohydrological processes: Merits, applications, and challenges. *Ecological Engineering*, 96, 137–149.

Ma, H., *et al*., 2023. A study on hydrological responses of the Fuhe River Basin to combined effects of land use and climate change. *Journal of Hydrology: Regional Studies*, 48, 101476.

Marhaento, H., Booij, M. J., and Hoekstra, A. Y., 2018. Hydrological response to future land-use change and climate change in a tropical catchment. *Hydrological Sciences Journal*, 63 (9), 1368–1385.

Nazeer, A., *et al*., 2022. Changes in the hydro-climatic regime of the Hunza Basin in the Upper Indus under CMIP6 climate change projections. *Scientific Reports*, 12 (1), 21442.

NHI, 2008. *Nederlands hydrological instrumentation model reporting: Sub-report crop characteristics*. Netherlands: Nederlands Hydrologisch Instrumentarium.

Papaioannou, G., *et al*., 2018. An operational method for flood directive implementation in ungauged urban areas. *Hydrology*, 5 (2), 24.

Philip, S. Y., *et al*., 2020. Regional differentiation in climate change induced drought trends in the Netherlands. *Environmental Research Letters*, 15 (9), 094081.

Popescu, I., 2013. *Theoretical background: Unsteady flow, in floods in a changing climate inundation modelling*. New York: Cambridge University Press, 21–30.

Rajib, A., *et al*., 2018. Hydrologic model predictability improves with spatially explicit calibration using remotely sensed evapotranspiration and biophysical parameters. *Journal of Hydrology*, 567, 668–683.

Ran, Q., *et al*., 2022. The relative importance of antecedent soil moisture and precipitation in flood generation in the middle and lower Yangtze River basin. *Hydrol. Earth Syst. Sci.*, 26 (19), 4919–4931.

Refsgaard, C. J., Storm, B., and Clausen, T., 2010. Système Hydrologique Europeén (SHE): review and perspectives after 30 years development in distributed physically-based hydrological modelling. *Hydrology Research*, 41 (5), 355–377.

Richards, L. A., 1931. Capillary conduction of liquids through porous mediums. *Physics*, 1 (5), 318–333.

Rigby, A. M., *et al*., 2022. LUCST: A novel toolkit for Land Use Land Cover change assessment in SWAT+ to support flood management decisions. *Environmental Modelling & Software*, 156, 105469.

Rossi, L., *et al*., 2023. European drought risk atlas.

Roy, B., and Rahman, M. Z., 2023. Spatio-temporal analysis and cellular automata-based simulations of biophysical indicators under the scenario of climate change and urbanization using artificial neural network. *Remote Sensing Applications: Society and Environment*, 31, 100992.

Sassi, M., *et al*., 2019. Impact of climate change on European winter and summer flood losses. *Advances in Water Resources*, 129, 165–177.

Sinha, R. K., Eldho, T. I., and Subimal, G., 2020. Assessing the impacts of land use/land cover and climate change on surface runoff of a humid tropical river basin in Western Ghats, India. *International Journal of River Basin Management*, 21 (2), 141–152.

Song, Y. H., Chung, E. S., and Shahid, S., 2021. Spatiotemporal differences and uncertainties in projections of precipitation and temperature in South Korea from CMIP6 and CMIP5 general circulation model s. *International Journal of Climatology*, 41 (13), 5899–5919.

Sorribas, M. V., *et al*., 2016. Projections of climate change effects on discharge and inundation in the Amazon basin. *Climatic Change*, 136 (3), 555–570.

Sunde, M. G., *et al*., 2017. Integrating downscaled CMIP5 data with a physically based hydrologic model to estimate potential climate change impacts on streamflow processes in a mixed-use watershed. *Hydrological Processes*, 31 (9), 1790–1803.

Thompson, J. R., *et al*., 2004. Application of the coupled MIKE SHE/MIKE 11 modelling system to a lowland wet grassland in southeast England. *Journal of Hydrology*, 293 (1), 151–179.

Tirupathi, C., and Shashidhar, T., 2020. Investigating the impact of climate and land-use land cover changes on hydrological predictions over the Krishna river basin under present and future scenarios. *Science of the Total Environment*, 721, 137736.

Trang, N. T. T., *et al*., 2017. Evaluating the impacts of climate and land-use change on the hydrology and nutrient yield in a transboundary river basin: A case study in the 3S River Basin (Sekong, Sesan, and Srepok). *Science of the Total Environment*, 576, 586–598.

van Dorland, R., *et al*., 2023. *KNMI national climate scenarios 2023 for the Netherlands*. De Bilt: Royal Netherlands Meteorological Institute.

van Genuchten, M. T., 1980. A closed-form equation for predicting the hydraulic conductivity of unsaturated soils. *Soil Science Society of America Journal*, 44 (5), 892–898.

Van Huijgevoort, M. H., *et al*., 2020. Influence of climate and land use change on the groundwater system of the Veluwe, The Netherlands: A historical and future perspective. *WATER*, 12 (10), 2866.

van Vliet, M. T. H., *et al*., 2012. A multi-model ensemble of downscaled spatial climate change scenarios for the Dommel catchment, Western Europe. *Climatic Change*, 111 (2), 249–277.

Vázquez, R., et al., 2002. Effect of grid size on effective parameters and model performance of the MIKE-SHE code. *Hydrological Processes*, 16 (2), 355–372.

Vernes, R., *et al*., 2005. Van gidslaag naar hydrogeologische eenheid: toelichting op de totstandkoming van de dataset REGIS II.

Viera, A. J., and Garrett, J. M., 2005. Understanding interobserver agreement: the kappa statistic. *Family Medicine*, 37 (5), 360–363.

Visser, A., *et al*., 2012. Climate change impacts on the leaching of a heavy metal contamination in a small lowland catchment. *Journal of Contaminant Hydrology*, 127 (1-4), 47–64.

VMM, n.d. Vlaamse Milieumaatschappij (Flemish Environment Agency) portal: Vlaanderen \ Waterinfo [online]. Available from: https://www.waterinfo.be/Themas#item=rainfall/more%20information/gauged%20rainfall [Accessed 27 November 2023].

Wedajo, G. K., Muleta, M. K., and Awoke, B. G., 2022. Impacts of combined and separate land cover and climate changes on hydrologic responses of Dhidhessa River basin, Ethiopia. *International Journal of River Basin Management*, 22 (1), 57–70.

Whitford, A. C., *et al*., 2023. A gauge-based sub-daily extreme rainfall climatology for western Europe. *Weather and Climate Extremes*, 41, 100585.

Witter, V. J., and Raats, T., 2001. Hydrological criteria for durable water systems. In: A. H. Schumann, *et al*., ed. *Regional management of water resources*. IAHS PUBLICATION, 231–238.

Wösten, J., *et al*., 1999. Development and use of a database of hydraulic properties of European soils. *Geoderma*, 90 (3-4), 169–185.

Yan, R., *et al*., 2019. Hydrological responses to climate and land use changes in a watershed of the Loess Plateau, China. *Sustainability*, 11 (5), 1443.

Yang, N., *et al*., 2020. Analysis of event-based hydrological processes at the hydrohill catchment using hydrochemical and isotopic methods. *Proc. IAHS*, 383, 99–110.

Ye, C., *et al*., 2023. Coupled effects of future rainfall and land use on urban stormwater drainage system in Tampa, Florida (USA). *Ecological Indicators*, 153, 110402.

Zhang, Y., *et al*., 2018. Understanding coastal wetland hydrology with a new regional-scale, process-based hydrological model. *Hydrological Processes*, 32 (20), 3158–3173.

Zhang, H., *et al*., 2020. Using an improved SWAT model to simulate hydrological responses to land use change: A case study of a catchment in tropical Australia. *Journal of Hydrology*, 585, 124822.

Zhang, Y., He, Y., and Song, J., 2023. Effects of climate change and land use on runoff in the Huangfuchuan Basin, China. *Journal of Hydrology*, 626, 130195.

Zhou, Q., *et al*., 2019. Comparison of urbanization and climate change impacts on urban flood volumes: importance of urban planning and drainage adaptation. *Science of the Total Environment*, 658, 24–33.